Studies on the Radiation Damage to Silicon Detectors For Use in the D0 Run2b Experiment

$A.Bean^1, R.Demina^4, J.Gardner^1, C.Gerber^2, Z.Ke^3,$
$S.Korjanevsky^4, S.Lager^5, A.Leflat^6, F.Lehner^7, R.Lipton^3,$
$J.R.Lackey^3, M.Merkin^6, P.A.Rapidis^3, V.Rykalin^{3*}, L.Shabalina^2,$
$L.Stutte^3, B.Webber^3$

1. University of Kansas
2. University of Illinois at Chicago
3. Fermilab
4. Kansas State University
5. Stockholm University
6. Moscow State University
7. University of Zurich, Switzerland

June 10, 2002

Abstract

The D0 experiment plans on building a new silicon detector to allow collection of a total of $15fb^{-1}$ of data for Run2. The new Run2b silicon sensors must allow them to withstand radiation doses commensurate with this amount of data. Here, seven prototype Run2b silicon detectors are tested for radiation hardness by exposing them to proton-induced radiation. This is done at the radiation damage facility, using the Fermilab 8 GeV proton booster to expose the silicon to fluences up to 15 Mrad. Also, the stable fluence constant, g_c and the leakage current slope α are measured for four of the seven detectors.   * Now at Northern Illinois University

1 Introduction

The D0 detector started taking data with a silicon detector in March of 2001. This silicon detector, called the Silicon Microstrip Tracker (SMT), is part of a central tracking system that will allow for better b-quark tagging through improvement to the impact parameter resolution on each track. The SMT was originally built for a data run containing 2-4 fb^{-1} of data (so called Run2a). The detector was designed before constraints on the Higgs mass suggested that a longer run at the Tevatron could possibly allow for a discovery of the Higgs. Updated information implies that a data run of up to 15 fb^{-1} in each of D0 and CDF could provide meaningful limits on the Higgs mass.

The current SMT detector is built using mostly double-sided silicon devices that were designed to be biased up to voltages of around 200V. Our current understanding, is that we will be unable to fully deplete these devices due to radiation damage after about 2-4 fb^{-1} of data. This is especially true for the inner layers.

The D0 collaboration started planning for a new silicon detector to be built to replace the current SMT detector. For this Run2b silicon detector, we hope to improve the b-tagging performance of the Run2a silicon detector. Our design studies call for a 6 layer device that fits into the existing space for the Run2a detector. We will place the innermost layer as close to the beam as possible. This appears to imply a minimum radius of this layer at about 1.5cm. So in addition to the increased luminosity requirements for this detector, there are also increased requirements on the radiation hardness for these devices. The technical design report which is now available describes the design parameters for the detector. [1]

The most important radiation damage mechanism in silicon is the bulk damage due to the non-ionizing part of the energy loss. It causes changes in the doping concentration (and therefore depletion voltage), increased leakage current, and decreased charged collection efficiency. A general overview of radiation damage in silicon detectors can be found elsewhere. [2,3] Over the operating period of Run2b, the innermost sensors will be subject to a fluence of about 2×10^{14} equivalent 1 MeV neutrons per cm^2. [4] Seriously damaged detectors will require high bias voltages to operate efficiently. For the construction of the tracker for Run2b, we've proposed the use of AC-coupled, single-sided single-metal p^+ on n-bulk silicon devices with integrated polysilicon resistors. The D0 group conducted tests using the proton beam from the 8GeV booster radiation damage facility during the summer of 2001 on prototype detectors.

Measurements were made on prototype detectors that are to be placed as closed to the beam as possible (those for layer 0). At a radius of 1.5cm, the expectation is that for every inverse femtobarn of data taken there is approximately a 1 MRad dose in charged particles. As the expected lifetime of Run2b is $15 fb^{-1}$, we exposed the silicon to a total of 15 Mrads in units of 5 Mrads. After each irradiation, measurements of the depletion voltage and leakage current were taken. One goal of these tests was to make sure that the silicon will stay depleted and operating reliably over the entire course of Run2b. Another concern was the noise produced from leakage current. Leakage current tends to rise linearly with fluence

Figure 1: The booster beam area. The detectors are placed in the pink box to the right of Victor Rykalin. Above this, the beam passes through the square region and through the toroid at the right.

while noise rises with the square root of leakage current. The effects of increasing fluence can be countered by decreasing temperature. Therefore, it is important to know what cooling temperature is needed to keep an acceptable signal to noise ratio.

2 Description of the Measurements

We used the Radiation Damage Facility, located in the Fermilab 8 GeV proton booster area to study radiation effects with prototype D0 Run2b detectors. Both tests to understand the current Run2a detectors and tests on prototype radiation hard detectors for Run2b have been done. The tests for the Run2a detectors are described elsewhere. [5, 6]

The proton beam produces a series of pulses which irradiate the detectors positioned in the beam path. See Figure 1 for a picture of the beam area. Pulses distribute protons in a two dimensional gaussian shape with an approximate full-width of 2.5 cm. Due to the relatively small diameter of the booster beam, the detectors must be moved with respect to the beam in a manner which exposes the entire surface as uniformly as possible. Therefore, the samples were mounted inside a temperature controlled box attached to a moving table which was moved in 0.5cm steps as shown in Figure 2. Remote controllers allow operation of this table in room TGS-102 outside of the radiation area as shown in Figure 3.

The delivered particle fluence was monitored with a Pearson 3100 toroid as shown in Figure 4. The toroid is calibrated to measure the number of protons passing though per count. With the beam intensity

3

Figure 2: The moving box used to move the detectors through the beam.

Figure 3: Room TGS-102 located outside of the radiation area with the data acquisition setup.

Figure 4: The Pearson 3100 Toroid which was used to monitor the particle fluence.

of 3×10^{11} per spill and a repetition rate of 3 seconds, the corresponding flux was 3×10^{11} protons per square centimeter per second. Activated aluminum foils were also used in calibrating the fluence monitoring. These showed that the proton flux was uniform over the irradiated area of the silicon detectors to within 20%. Figure 5 shows a picture of the silicon after irradiation.

Eight silicon detectors were exposed to 15 Mrads in increments of 5 Mrads. Each of the sensors was made using a 300μm thick sensor. The expected size of the Run2b L0 sensors are an active length of 76.7mm and an active width of 12.8mm. The readout pitch is 50μm with intermediate strips halfway in between. Three of the sensors tested were manufactured by Hamamatsu (HMM) that were spare L00 sensors from CDF's Run2a silicon detector. Their dimensions matched those for the Run2b L0 specifications. There were three sensors made by Elma in Russia with dimensions of 18×20 mm. These devices were oxygenated but at a level too low to affect the depletion voltage in a beneficial way. Also tested were other CDF L00 sensors: 1 made by ST in Catania, and one by Micron. Both of these sensors were oxygenated.

After each exposure, the silicon detectors were taken to the Silicon Detector Center for measurements of both depletion voltage and leakage current. Before the detectors were tested, they were allowed to anneal for a few days at $5°C$ and afterward were stored in a freezer at $-12°C$. An effort was made to limit the time spent outside of the freezer and to keep records of this. This is because detectors anneal quickly when not kept cold. For comparison, a detector at room temperature will anneal approximately 1000 times faster than when in the freezer. Annealing must be limited and kept track of, because it can greatly effect detector

Figure 5: One of the irradiated silicon detectors showing visually that full coverage by the beam across the sensor was achieved.

behavior. When out of the freezer, detectors not being tested were kept in a NO_2 chiller at $-12^{\circ}C$. Also, the chiller is used for varying the temperature at which measurements are made.

3   Depletion Voltage Measurements

In order to measure the depletion voltage, we used the laser teststand used to measure charge collection for the Run2a silicon detectors. [7] The detector is kept inside a dark box with only a hole large enough to fit a laser through. This near infrared laser of wavelength 1063nm is placed in the hole where it can hit the face of the silicon. The effect is to release charge which mostly passes through the aluminum readout strips and into the bulk of the silicon. With the laser attenuation length of 206μm, there was light traversing the entire 300μm thickness of the silicon. The spot size covers approximately a 20 readout strip full-width and is gaussian in shape. The output amplitude of the laser was adjusted for each measurement so that the preamplifier output was between 200 and 350mV. Figure 6 shows that the output amplitude is linear and does not affect the depletion voltage determination.

Using the relative output amplitude voltage measured in the center of the illuminated region plotted as a function of the bias voltage, the depletion voltage can be determined. The depletion voltage in these plots is at the first applied bias voltage where the output amplitude measurement plateaus. Determining the depletion voltage from these plots can be highly subjective. Therefore, it is important to have a consistent method for measuring it. First, a diagonal line is fitted by hand to the rising out-

6
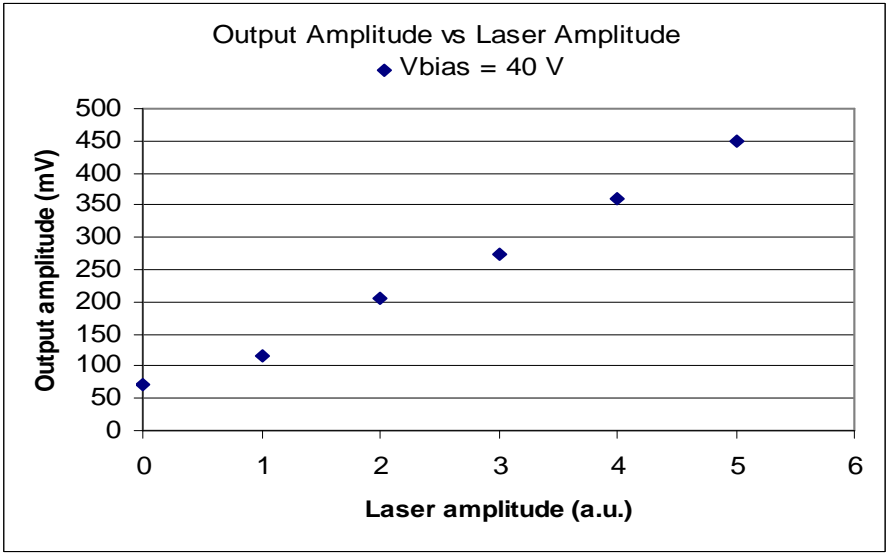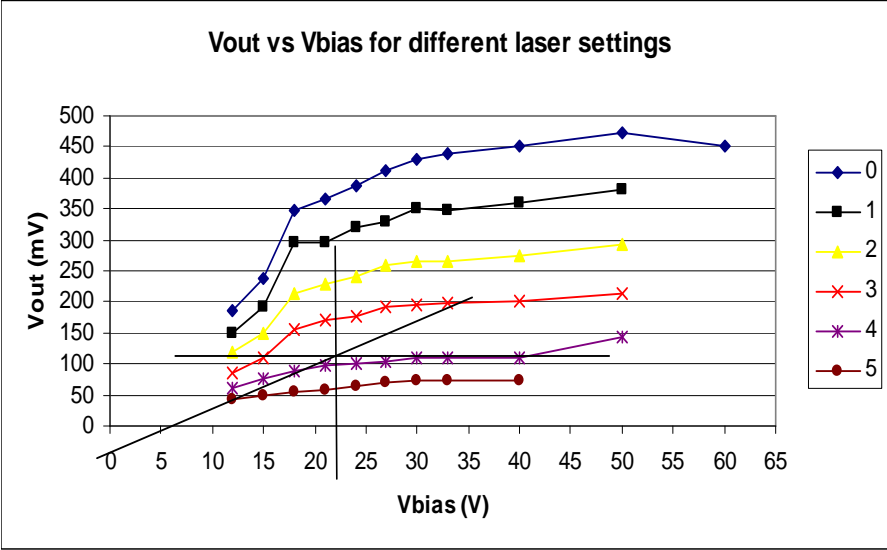
Figure 6: Plots showing the effects of laser amplitude on output amplitude. The top plot is of output amplitude vs bias voltage at 6 increasingly intense laser settings and the bottom plot demonstrates the linear dependence of output amplitude on laser amplitude.

7

	depletion voltage (V_{dep})			
detector	0 Mrad	5 Mrad	10 Mrad	15 Mrad
Hamamatsu 0077	62±10	255±40	300±40	400±70
Hamamatsu 0134	75±30	285±30	325±40	440±30
Hamamatsu 0144	33±10	none	290±35	none
Elma 233	30±10	180±50	250±25	none
Elma 236	28±8	250±40	260±30	none
Elma 253	27±5	170±50	275±40	610±70
Micron 1462 4c	98±20	265±50	350±20	370±40
ST230W2D6	140 ± 20	140 ± 20	280 ± 50	none

Table 1: Depletion voltage data for detector prototypes before irradiation, and after 5, 10, and 15 Mrad measured in Volts.

put amplitude data. if there is a second smaller slope before the plateau, then that slope is used. Second, a line is fitted to the plateau. This line is ideally horizontal, but may in reality have a small positive slope. The majority of the error in determining the depletion voltage is assumed to be from variances found using this method. These variances are found by altering both the line estimating the rising output amplitude and the line fitted to the plateau. There is typically a fair amount of leeway when fitting straight lines to the data. To find a minimum possible depletion voltage both the the rising output amplitude and plateau lines are altered to give a minimum conceivable depletion and the opposite for a maximum bound. Figure 7 shows an example of this procedure using Hamamatsu 0077 at 10 Mrads. The error range is approximated as symmetric: $\pm (max - min)/2$.

Each detector was tested before irradiation and after each irradiation burst ideally producing four depletion voltage determinations as a function of fluence. Table 1 gives the depletion voltage determinations for each one of the sensors tested and Figure 8 summarizes these measurements. Initially, a bias supply capable of supplying only 400V was used. For the third exposure which brought the total radiation level to 15 Mrad, only four of the original detectors were able to be depleted satisfactorily with our bias supplies which were then capable of providing up to 800V. Hamamatsu 0077 and Hamamatsu 0134 had depletion voltages of about 400V, Elma 253 had $V_{dep} = 610V$, and Micron 1462 4c had $V_{dep} = 370V$. Figure 9, Figure 10, Figure 11, Figure 12, Figure 13, Figure 14, Figure 15, and Figure 16 show the output amplitude as a function of applied bias voltage from which the depletion voltages were determined. At high radiation levels especially, it can be very difficult to determine precisely at what voltage a detector depletes. Generally, in output amplitude vs. bias voltage plots, the output amplitude more or less steadily increases until it reaches a plateau. At this point the output amplitude should stop increasing, however many times it will continue increasing although at a smaller rate. Also, it is possible for the slope of output amplitude to depletion to change before being fully depleted.

8

HAM.0077: Depletion Voltage at 10 Mrad

Min = 260V   Max = 340V

Output amplitude (mV)
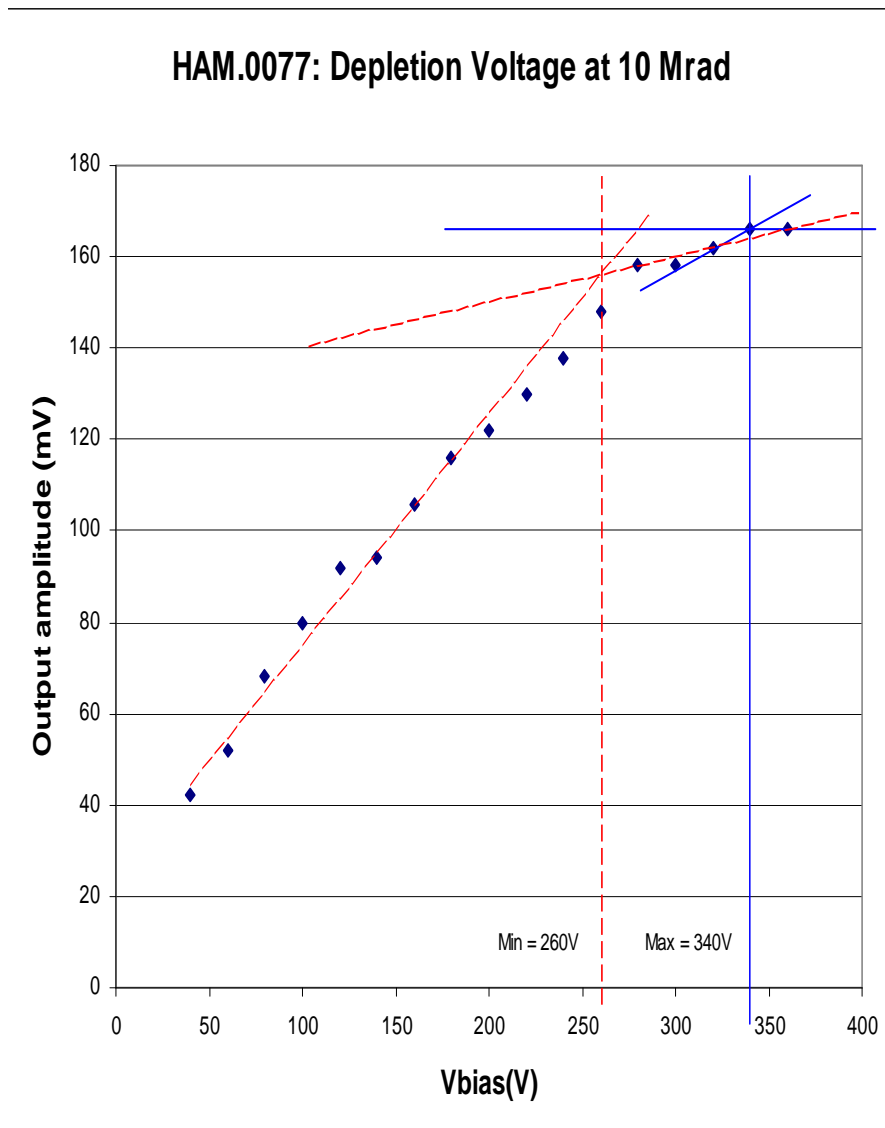
Vbias(V)

Figure 7: Example for determining the depletion voltage and its errors for the Hamamatsu 0077 detector at 10 Mrad. The output amplitude is plotted versus applied bias voltage. The leftmost vertical line (dotted) shows the minimum bias voltage found while the rightmost vertical line shows the maximum.

Depletion Vs. Fluence

- ◆ ELMA 253
- ■ ELMA 236
- ▲ ELMA 233
- ✕ Micron 1462 4c
- □ HAM.0144
- ● HAM.0077
- △ HAM.0134
- ▬ ST-230W2D6
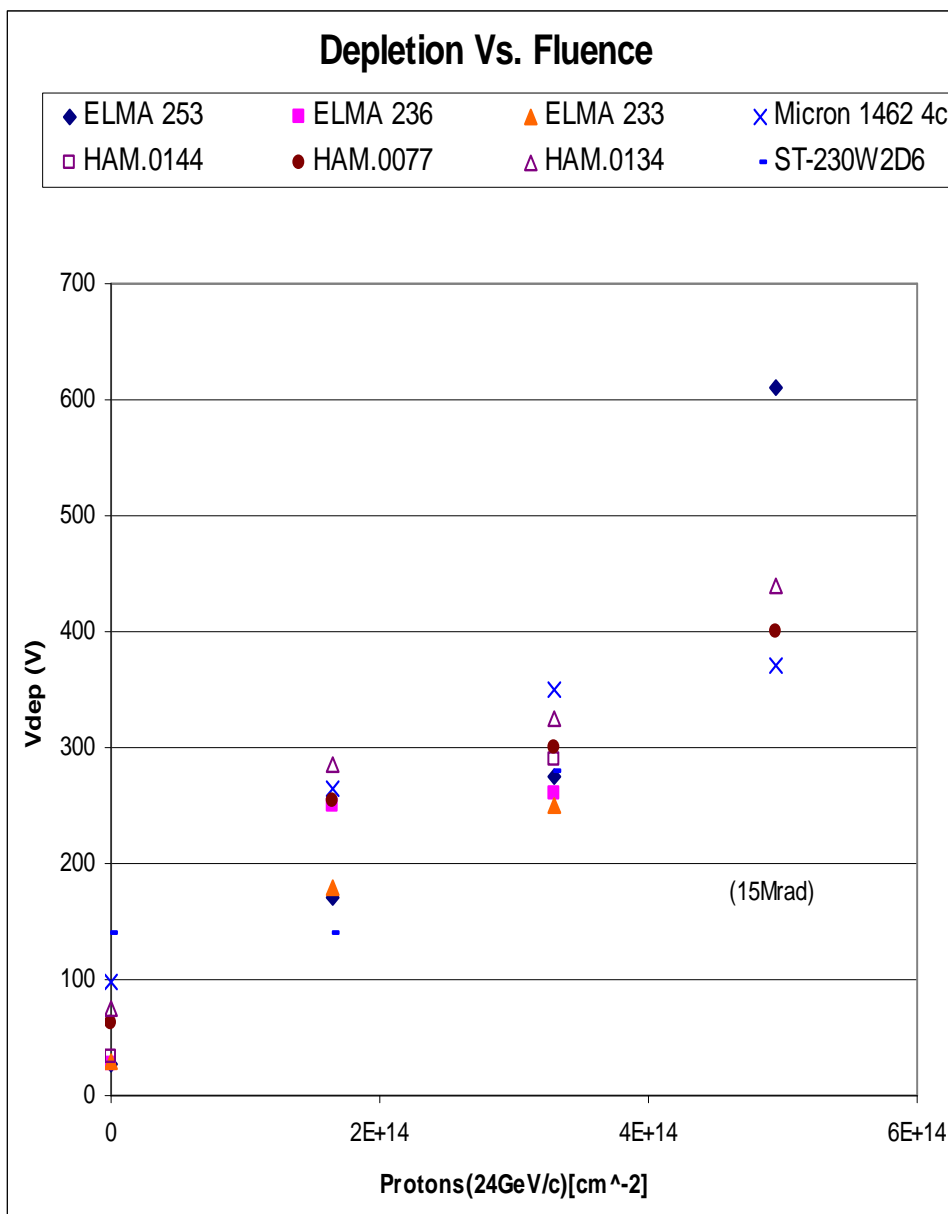
Figure 8: Plot of depletion voltage versus fluence for all detectors tested.
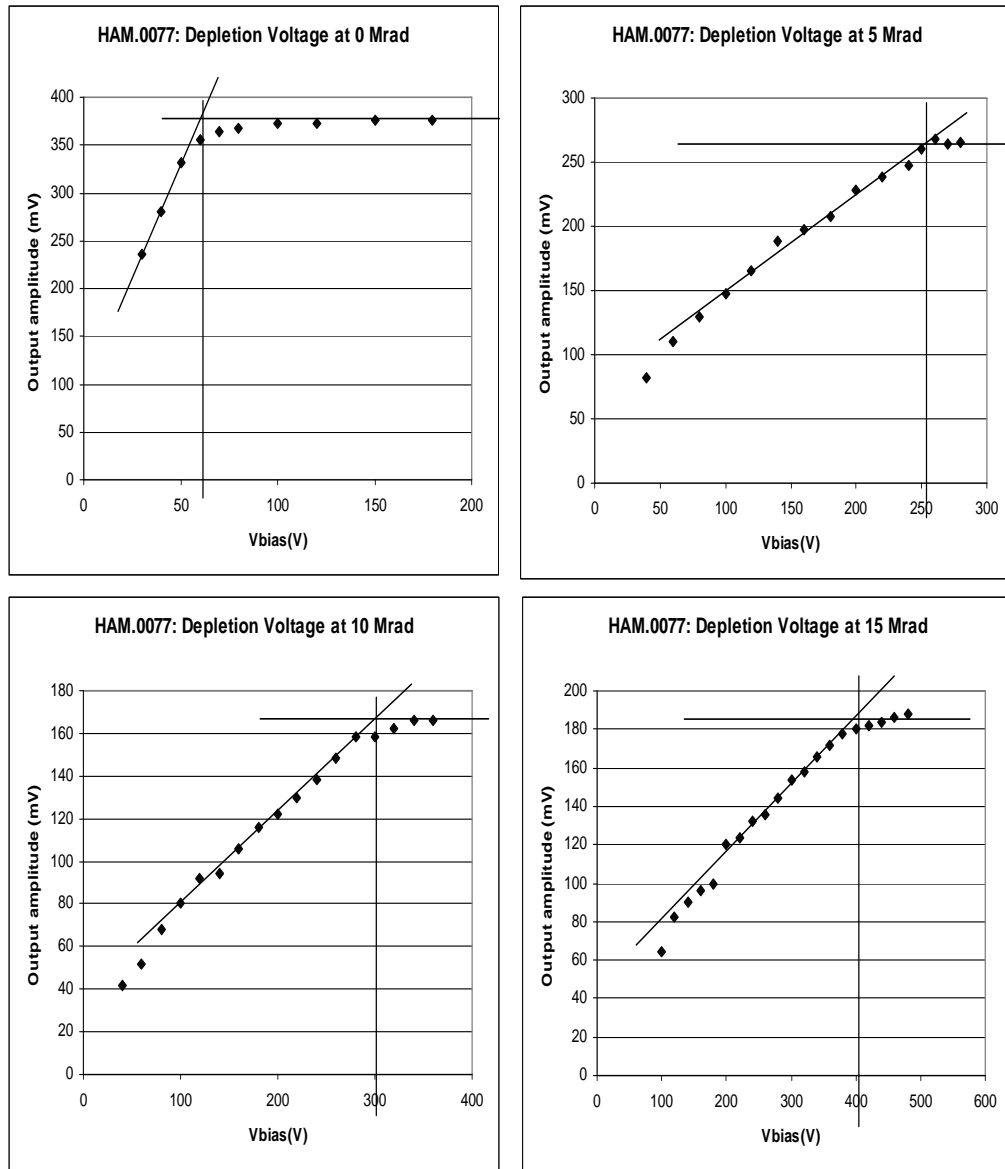
Figure 9: Plots of the output amplitude versus applied bias voltage to determine the depletion voltage for Hamamatsu 0077. The plots shown are: Top Left (before irradiation), Top Right (5 MRad), Bottom Left (10 MRad), Bottom Right (15 MRad).
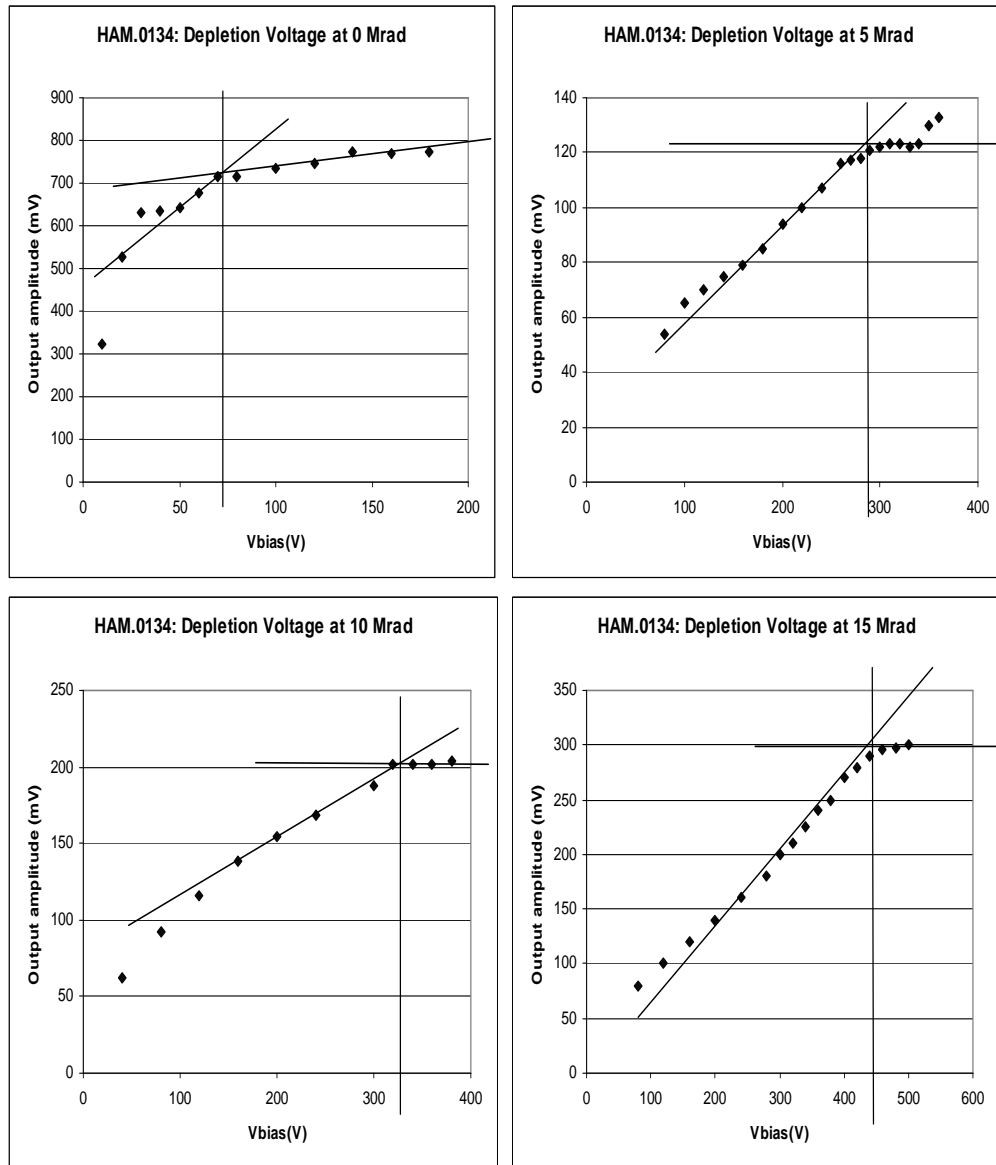
Figure 10: Plots of the output amplitude versus applied bias voltage to determine the depletion voltage for Hamamatsu 0134. The plots shown are: Top Left (before irradiation), Top Right (5 MRad), Bottom Left (10 MRad), Bottom Right (15 MRad).
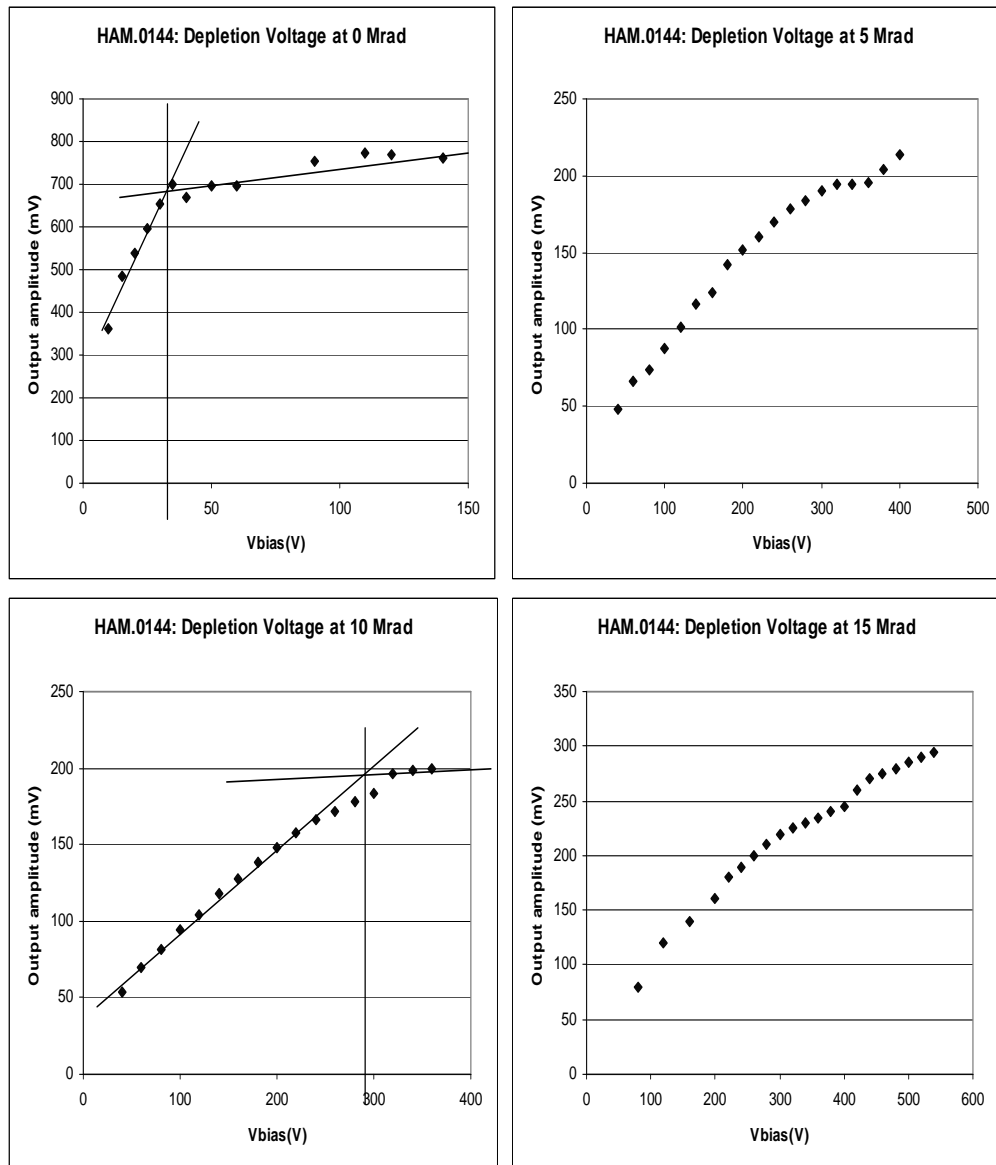
Figure 11: Plots of the output amplitude versus applied bias voltage to determine the depletion voltage for Hamamatsu 0144. The plots shown are: Top Left (before irradiation), Top Right (5 MRad), Bottom Left (10 MRad), Bottom Right (15 MRad).

13
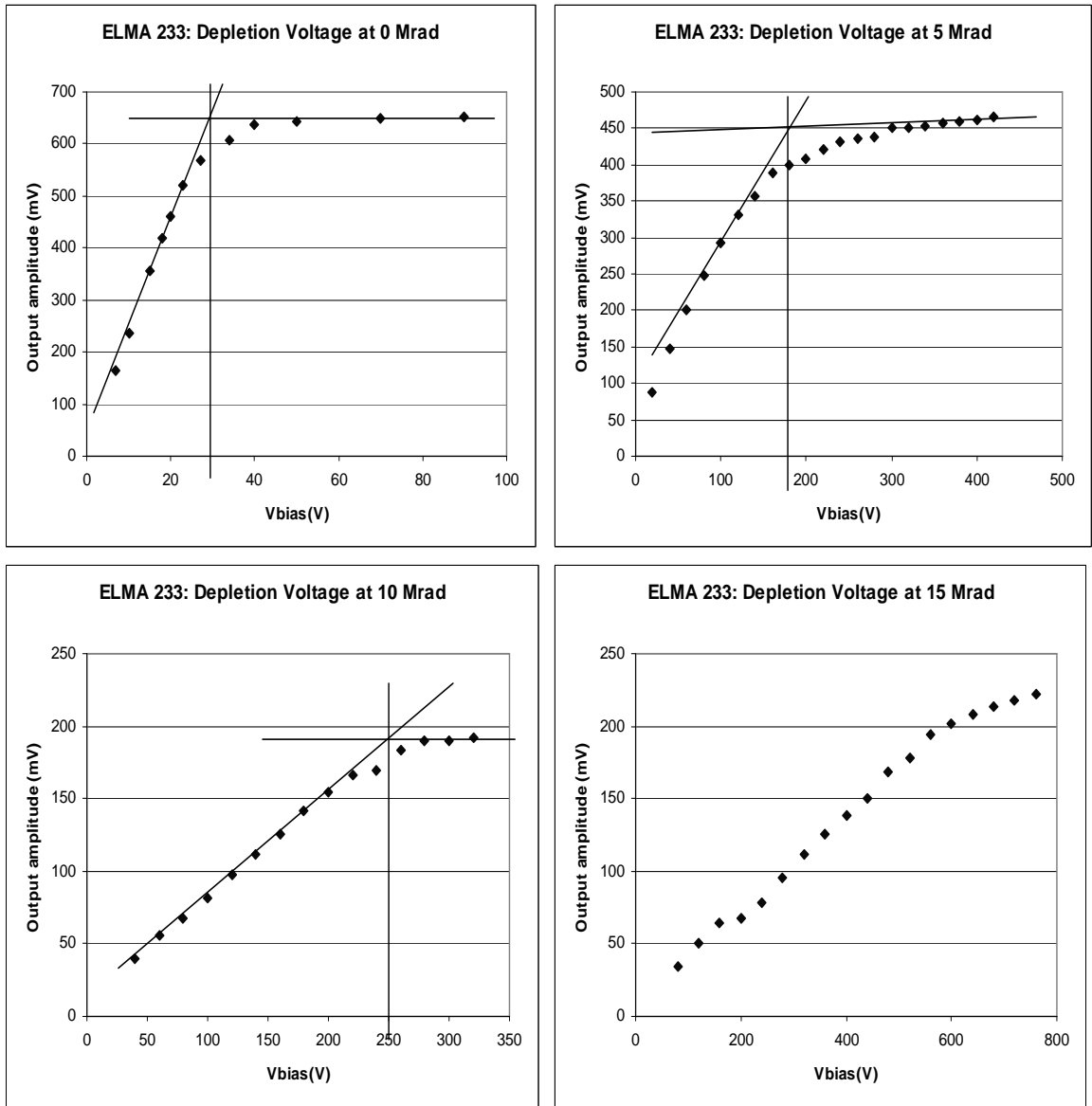
Figure 12: Plots of the output amplitude versus applied bias voltage to determine the depletion voltage for Elma 233. The plots shown are: Top Left (before irradiation), Top Right (5 MRad), Bottom Left (10 MRad), Bottom Right (15 MRad).
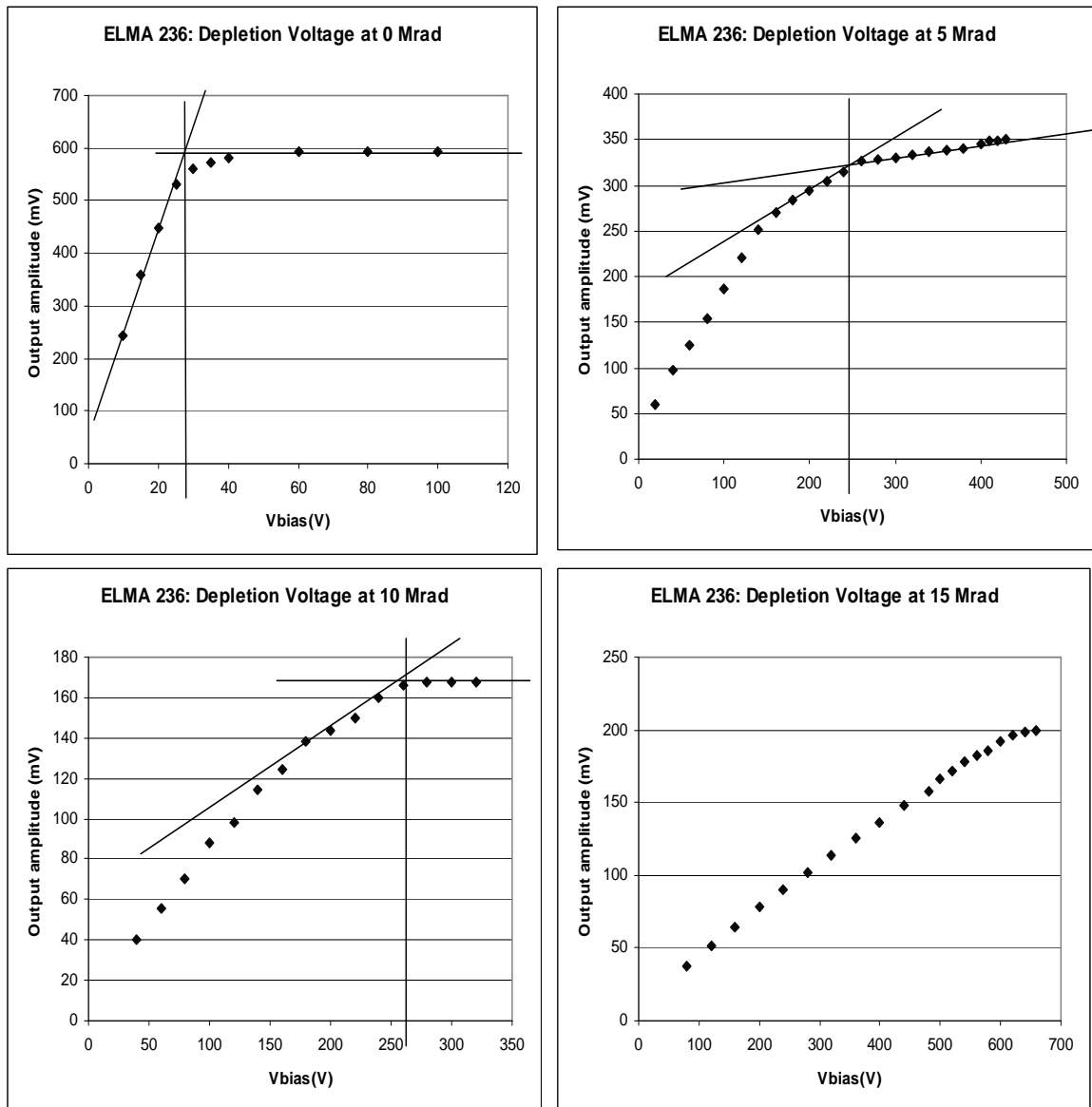
Figure 13: Plots of the output amplitude versus applied bias voltage to determine the depletion voltage for Elma 236. The plots shown are: Top Left (before irradiation), Top Right (5 MRad), Bottom Left (10 MRad), Bottom Right (15 MRad).
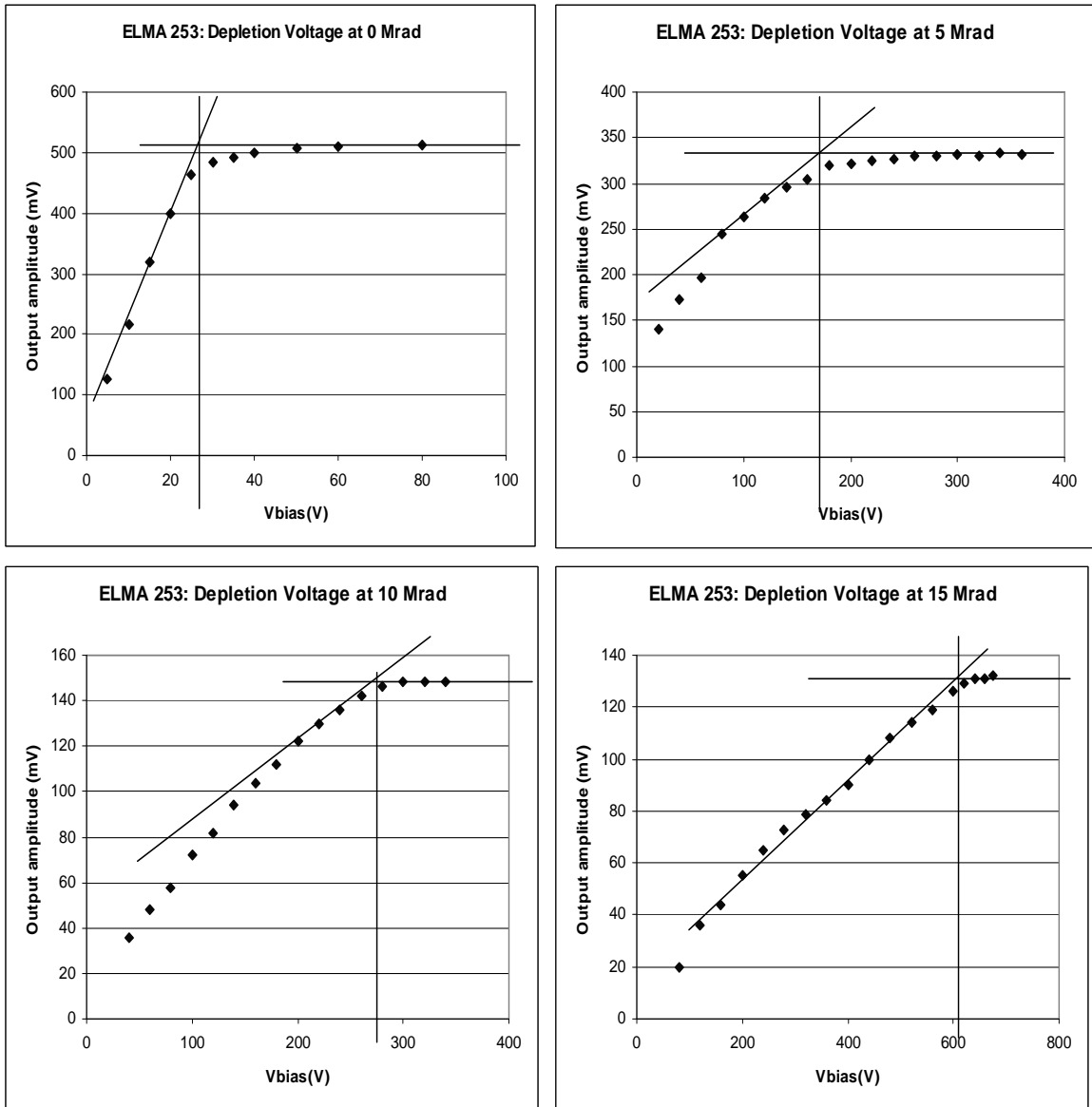
Figure 14: Plots of the output amplitude versus applied bias voltage to determine the depletion voltage for Elma 253. The plots shown are: Top Left (before irradiation), Top Right (5 MRad), Bottom Left (10 MRad), Bottom Right (15 MRad).
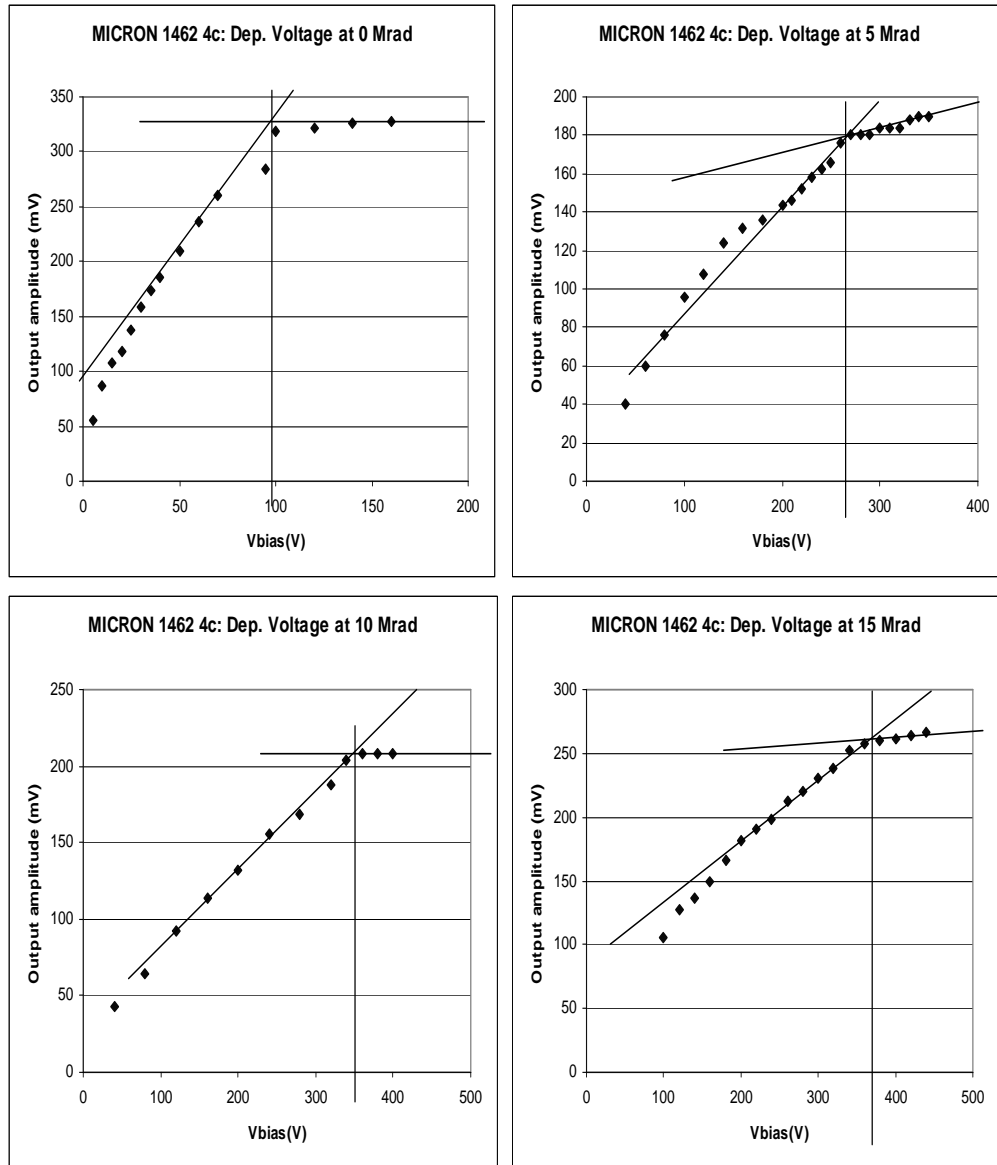
Figure 15: Plots of the output amplitude versus applied bias voltage to determine the depletion voltage for Micron 1462 4C. The plots shown are: Top Left (before irradiation), Top Right (5 MRad), Bottom Left (10 MRad), Bottom Right (15 MRad).
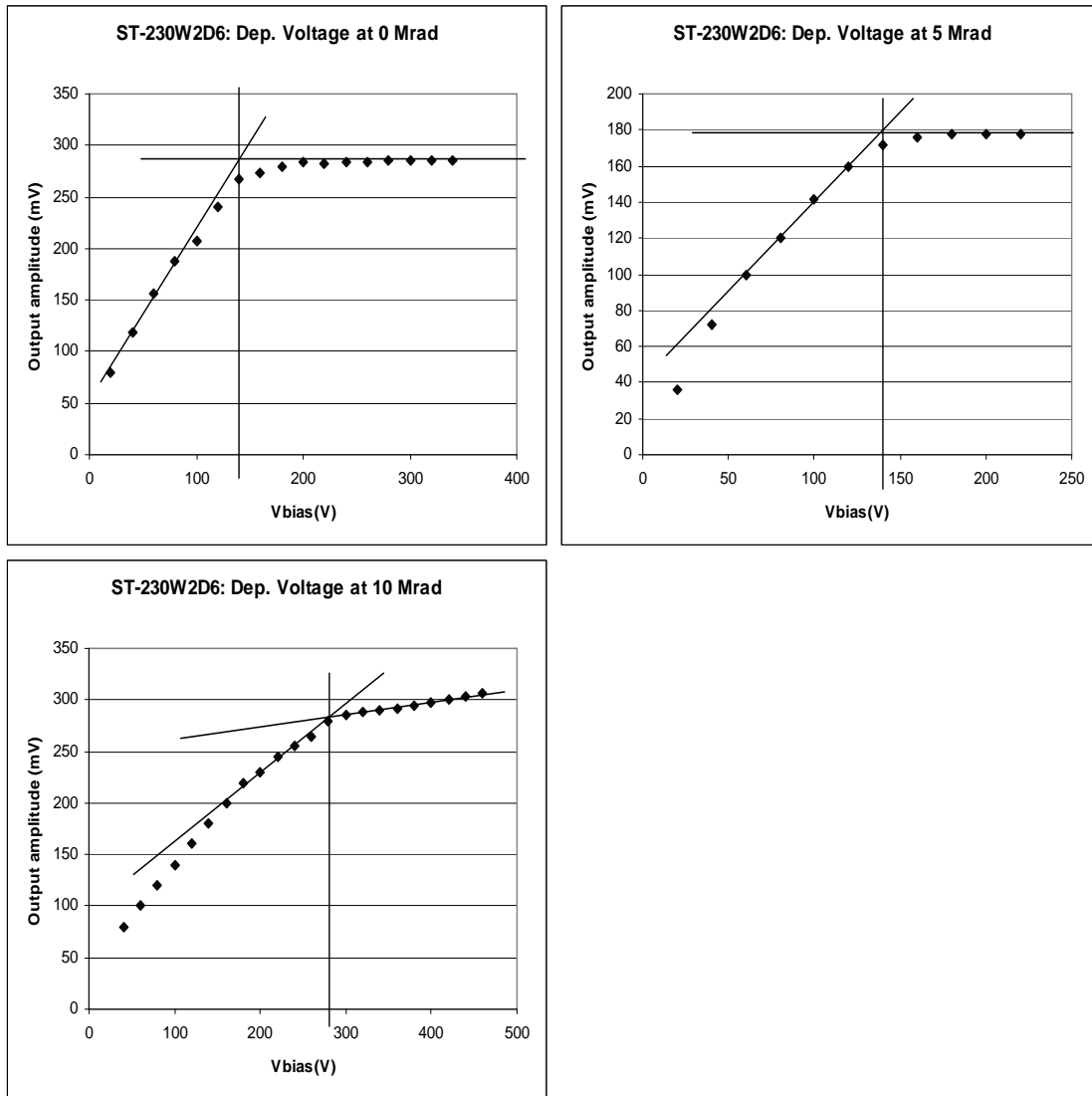
Figure 16: Plots of the output amplitude versus applied bias voltage to determine the depletion voltage for ST230W2D6. The plots shown are: Top Left (before irradiation), Top Right (5 MRad), Bottom Left (10 MRad), Bottom Right (15 MRad).

The depletion voltage measurements are consistent with our expectations and show that the detectors will be able to be biased with our anticipated radiation dose for Run2b. Improvements can be made in tests for the future if a power supply is obtained that will allow for a higher voltage range to be probed for the initial measurements. By plotting the output voltage for a range above the seen depletion voltage, the systematic error in the determination of the voltage could be reduced.

4   Leakage Current Measurements

We measured the leakage current as a function of bias voltage before irradiation and after each irradiation step. The amount of noise produced is proportional to the square root of leakage current. Therefore, if the leakage current is too high, the signal to noise ratio will drop below acceptable limits.

Leakage current is heavily dependent on fluence and temperature. This relation can be approximated with Equation 1.

$$\frac{I_{lkg2}}{I_{lkg1}} = (\frac{T_2}{T_1})^2 \ exp(\frac{-E_g}{2k_b} \ \frac{(T_1 - T_2)}{T_1 \ T_2}) \ \frac{\Phi_2}{\Phi_1} \tag{1}$$

Here, T is temperature in Kelvin, $E_g = 1.12$ eV, and $k_b = 8.614 * 10^{-5}$ eV/K. Equation 1 indicates that the leakage current should be related to fluence by a single constant. This constant is α in Equation 2.

$$I_{lkg} = \alpha \ \Phi \tag{2}$$

After a few days of annealing, we measured the leakage current. The leakage current is determined to be

$$I_{lkg} = \frac{V_{bias}}{R} \tag{3}$$

where R = 15 kohm is the value of the resistor through which the leakage current flows between V_{bias} and ground. See Figure 17 for a diagram.

Measurements were taken at two temperatures. It is important for the temperature to be known precisely throughout a leakage current vs. bias voltage measurement since small variations in temperature can significantly affect the shape of the plot. See Figure 18 for an example. Here we see that the temperature was varying by as much as $2^\circ C$ over the course of the measurement. For the low temperature measurements, the detectors were kept in the storage freezer at $-12^\circ C$. For higher temperature measurements, they were taken out and placed inside the chiller and read out using the burn-in stands used for Run2a were the temperatures were measured to be between $5 - 11^\circ$C. The measured leakage currents after 10 Mrads are shown in Figure 19. Here we see the measurements taken at both $-12^\circ C$ and $11^\circ C$ as a function of the bias voltage. Figure 20 shows the leakage currents measured after 15 Mrads for $5^\circ C$ and $-12^\circ C$.

We measured the leakage current for each of the detectors at V_{bias} = V_{dep} and approximately T = $-12^\circ C$ before irradiation and after 5, 10, and 15Mrads of irradiation. The leakage current measurements were
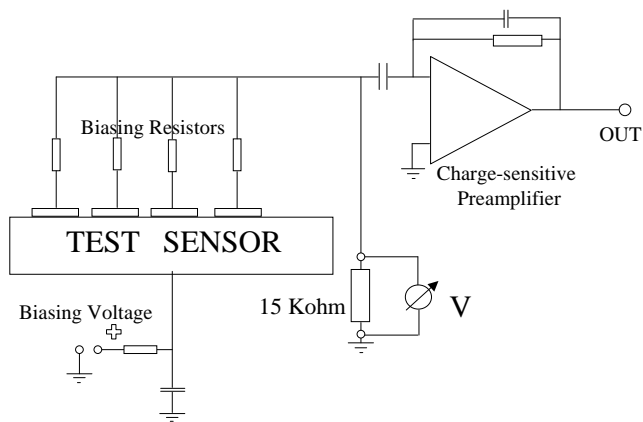
Figure 17: A schematic for the teststand at Si-Det. Leakage current is found through the voltage drop across the 15 kohm resistor. Output amplitude is measured from the voltage produced by a charge-sensitive preamplifier.
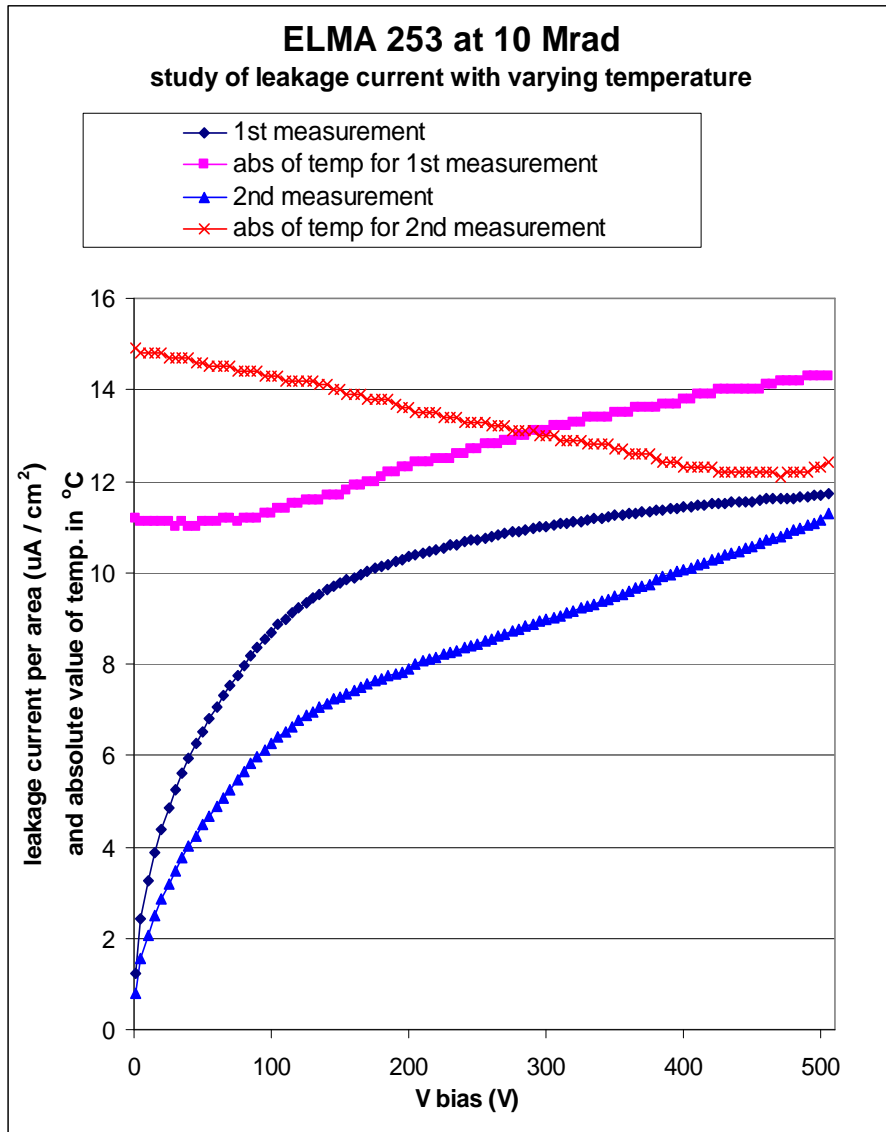
Figure 18: This plot demonstrates the dependence of leakage current on temperature using ELMA 253 at 10 Mrad. Both leakage current per area and the absolute value in $°C$ of the corresponding temperature of the sensor are recorded for 2 measurements taken at different times.
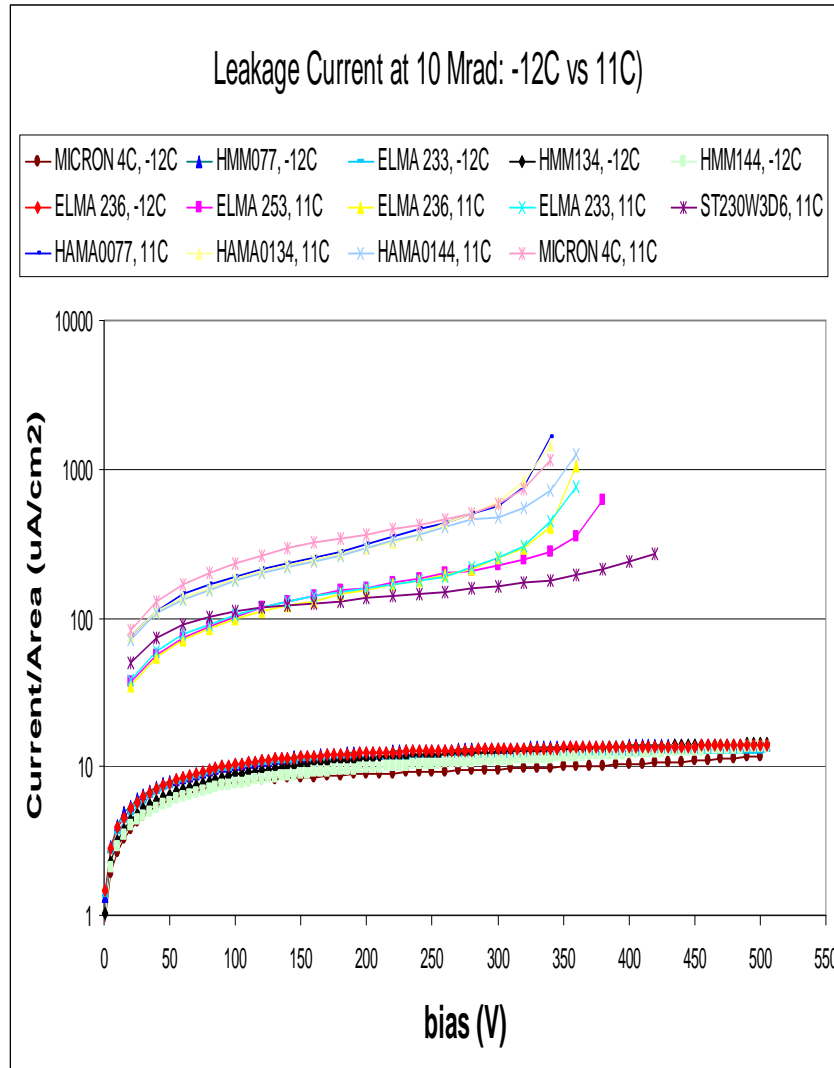
Figure 19: Leakage current per area measured as a function of bias voltage after 10Mrads of irradiation. Curves for the following sensors are given both at $-12°C$ and $11°C$: HAMA077, HAMA134, HAMA144, ELMA 233, ELMA 236, and Micron 4C. In addition, measurements for ELMA 253 and ST230W3D6 are shown for a temperature of $11°C$.
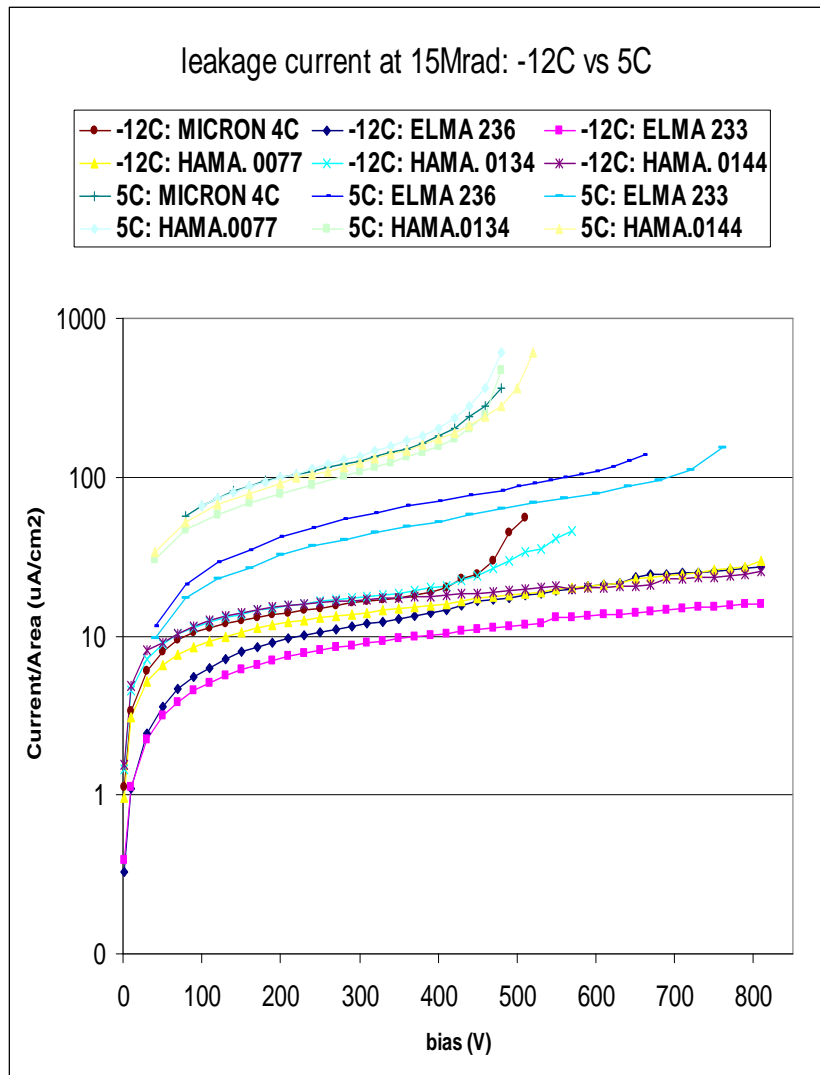
Figure 20: Leakage current per area measured as a function of bias voltage after 15Mrads of irradiation. Curves are shown both at $5°C$ and $-12°C$ for the following six sensors: Micron 4C, HAMA 077, HAMA 134 and HAMA 144, ELMA 233 and ELMA 236.

Irradiation (Mrad)	0 (nA/cm^2)	5 (mA/cm^2)	10 (mA/cm^2)	15 (mA/cm^2)
Hamamatsu 0077	3.3 ± 0.6	0.23 ± 0.13	0.27 ± 0.13	0.35 ± 0.14
Hamamatsu 0134	86 ± 15	0.17 ± 0.04	0.48 ± 0.18	0.32 ± 0.09
Hamamatsu 0144	35 ± 6	none	0.21 ± 0.04	none
Elma 233	1.04 ± 0.03	0.09 ± 0.02	0.14 ± 0.02	none
Elma 236	0.98 ± 0.04	0.10 ± 0.02	0.09 ± 0.02	none
Elma 253	5.0 ± 0.8	0.09 ± 0.02	0.16 ± 0.03	0.15 ± 0.04
Micron 1462 4c	27 ± 5	0.17 ± 0.04	0.6 ± 0.2	0.25 ± 0.06
ST230W2D6	0.22 ± 0.06	0.06 ± 0.01	0.09 ± 0.02	none

Table 2: Leakage current measured at the depletion voltage V_{dep} and normalized to a temperature of $T = 10°C$. (Note that leakage current units are in nA for 0 Mrad and mA for 5, 10 and 15 Mrad.)

normalized to $10°C$ using Equation 1. Figure 21 and Figure 22 show the leakage current as a function of applied bias voltage before irradiation. Figure 23, Figure 24, Figure 25, Figure 26, Figure 27, Figure 28, and Figure 29 show the leakage current as a function of bias voltage at each of the three radiation doses. Also on the graphs are vertical lines indicating the leakage current at the depletion voltage for each irradiation level. Table 2 gives the values of the leakage currents per area with their errors which are discussed below.

The main errors on these measurements are due to both the accuracy of the temperature determination, which was approximately $\pm 2°C$, and uncertainty in the depletion voltage. Uncertainty from T is found with a differential error estimate

$$\delta(I_{lkg}) \quad = \quad \frac{dI_{lkg}}{dT} \, \delta T \quad = \quad (\frac{2}{T} + \frac{E_g}{2k_B T^2}) \, I \, \delta T \tag{4}$$

which, for $\delta T = 2°C$ and $T = 10°C = 283$Kelvin, gives

$$\delta(I_{lkg}) \quad = \quad 0.17 \, I \tag{5}$$

Table 3 gives the errors on the leakage current measurement due to depletion voltage and temperature uncertainty. The expected noise and operating temperatures from these measurements is described in more detail in Reference [4].

Figure 23, Figure 24, Figure 25, Figure 26, Figure 27, Figure 28, Figure 29, and Figure 30 show the leakage current as a function of bias voltage after irradiation of 5Mrad, 10Mrad, and 15Mrad.

5 Determination of Radiation Damage Slope and Coefficient

With our depletion voltage measurements as a function of fluence, we attempt to fit for the radiation damage slope g_c. The stable fluence damage
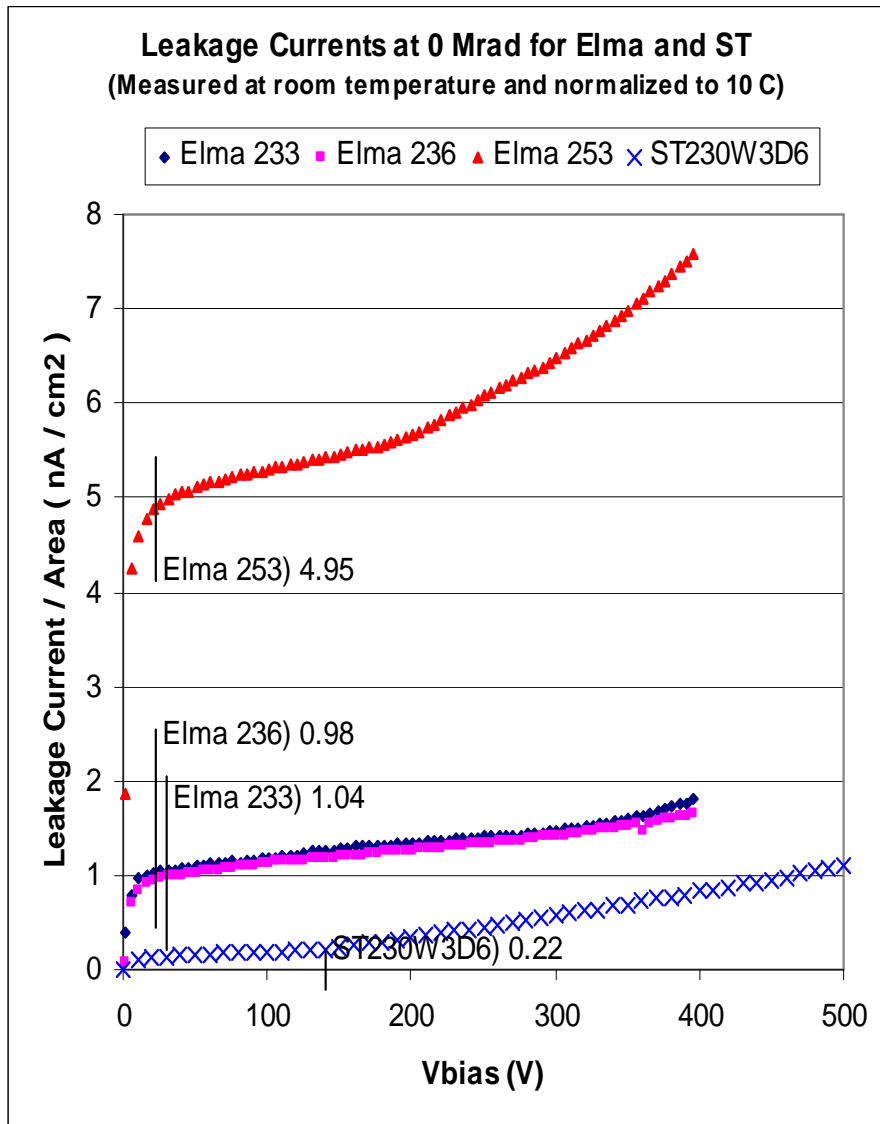
Figure 21: The leakage current per area measured as a function of applied bias voltage before irradiation for the ELMA233, ELMA236, ELMA253 and ST230W3D6 sensors. The vertical lines indicate the measured depletion voltages with the leakage current values listed beside them.

Leakage Currents at 0 Mrad for Ham. and Micron

(Measured at room temperature and normalized to 10 C)

- ◆ Hamamatsu 0077
- ■ Hamamatsu 0134
- ▲ Hamamatsu 0144
- ✕ Micron 1462 4c

Ham.0134) 85.8

Ham.0144) 34.8

Micron 1462 4c) 27.2

Ham.0077) 3.25

Leakage Current / Area (nA / cm2)
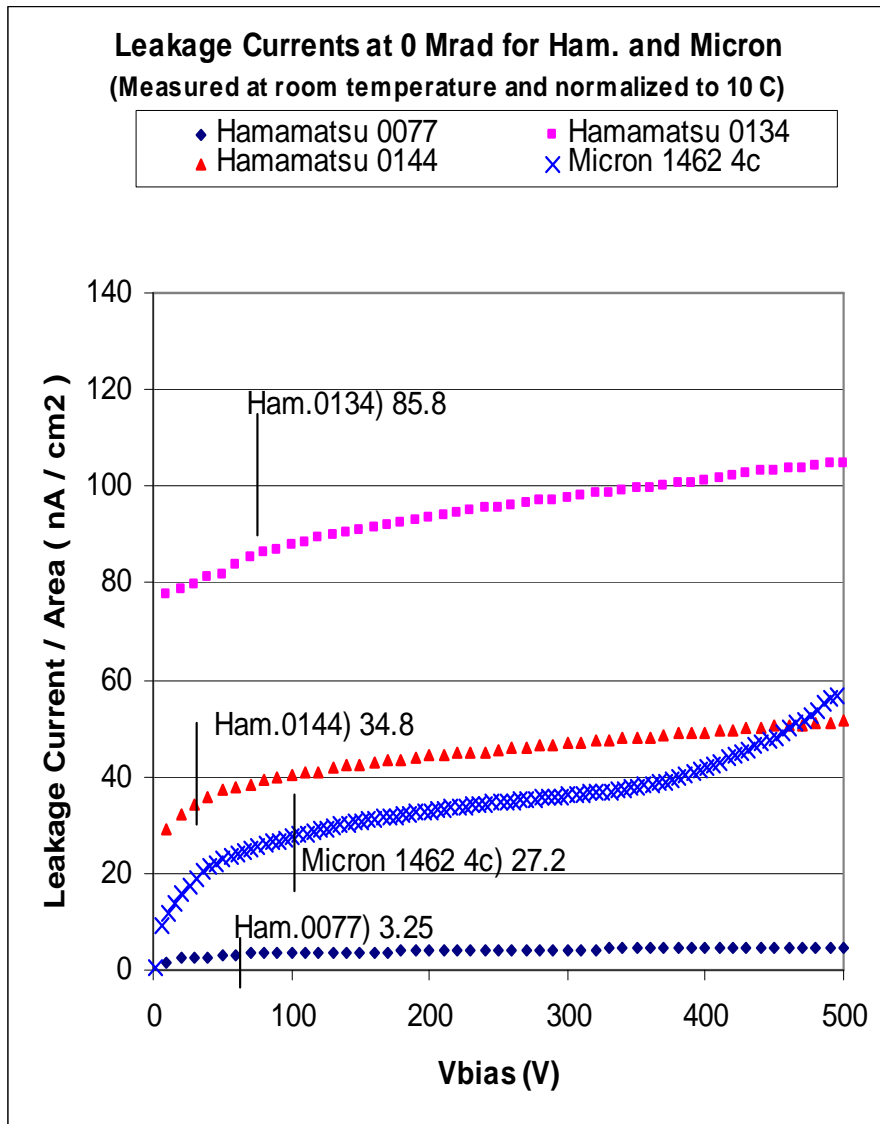
Vbias (V)

Figure 22: The leakage current per area measured as a function of applied bias voltage before irradiation for the HMM077, HMM0134, HMM0144 and MICRON 1462 4c sensors. The vertical lines indicate the measured depletion voltages with the leakage current values listed beside them.
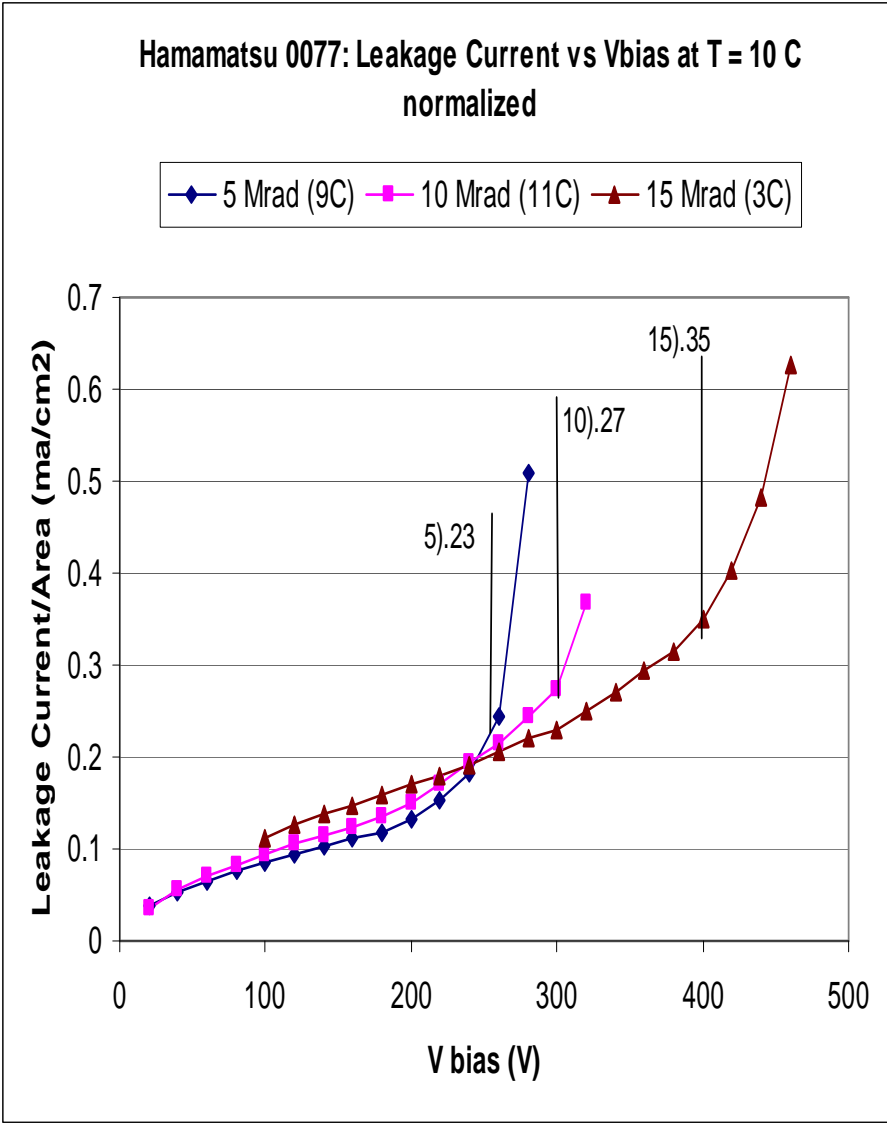
Figure 23: The leakage current per area measured as a function of applied bias voltage after irradiation of 5Mrad, 10Mrad, and 15Mrad for the HMM077 sensor. The vertical lines indicate the measured depletion voltages with the leakage current values listed beside them.
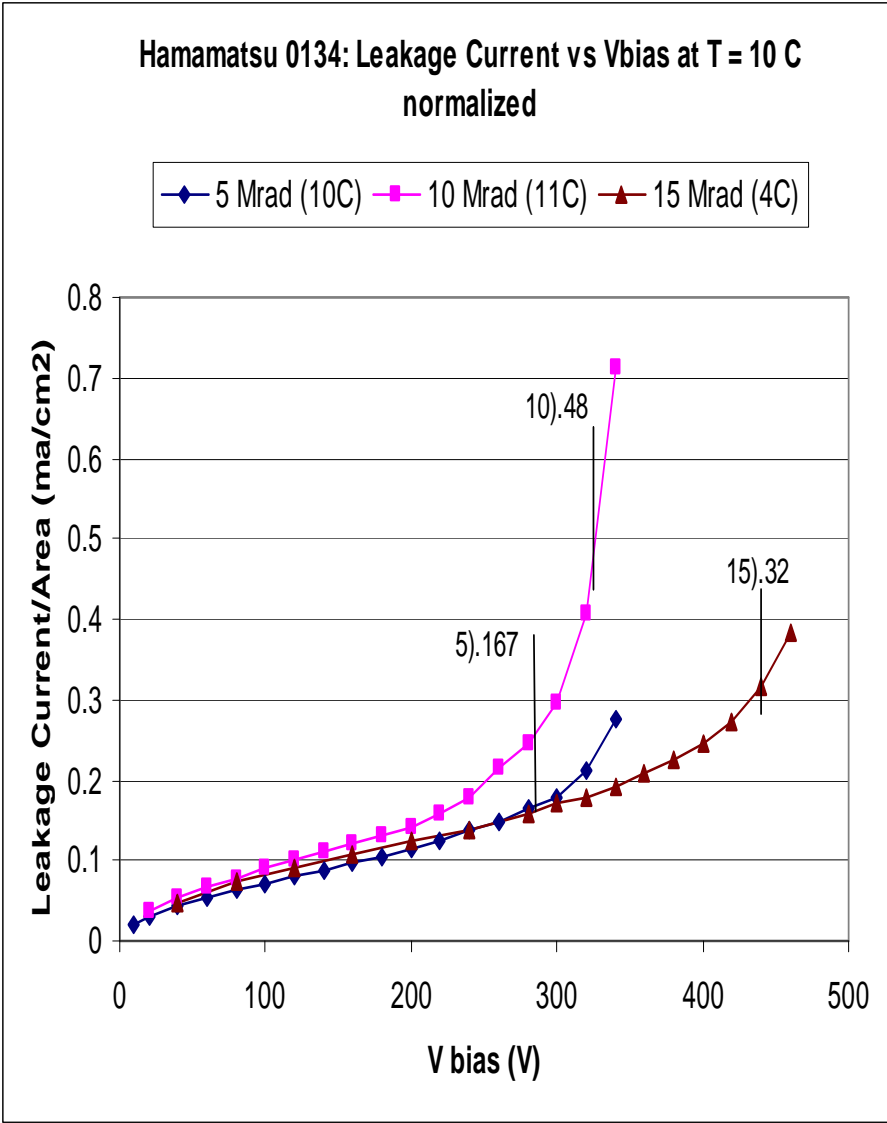
Figure 24: The leakage current per area measured as a function of applied bias voltage after irradiation of 5Mrad, 10Mrad, and 15Mrad for the HMM0134 sensor. The vertical lines indicate the measured depletion voltages with the leakage current values listed beside them.
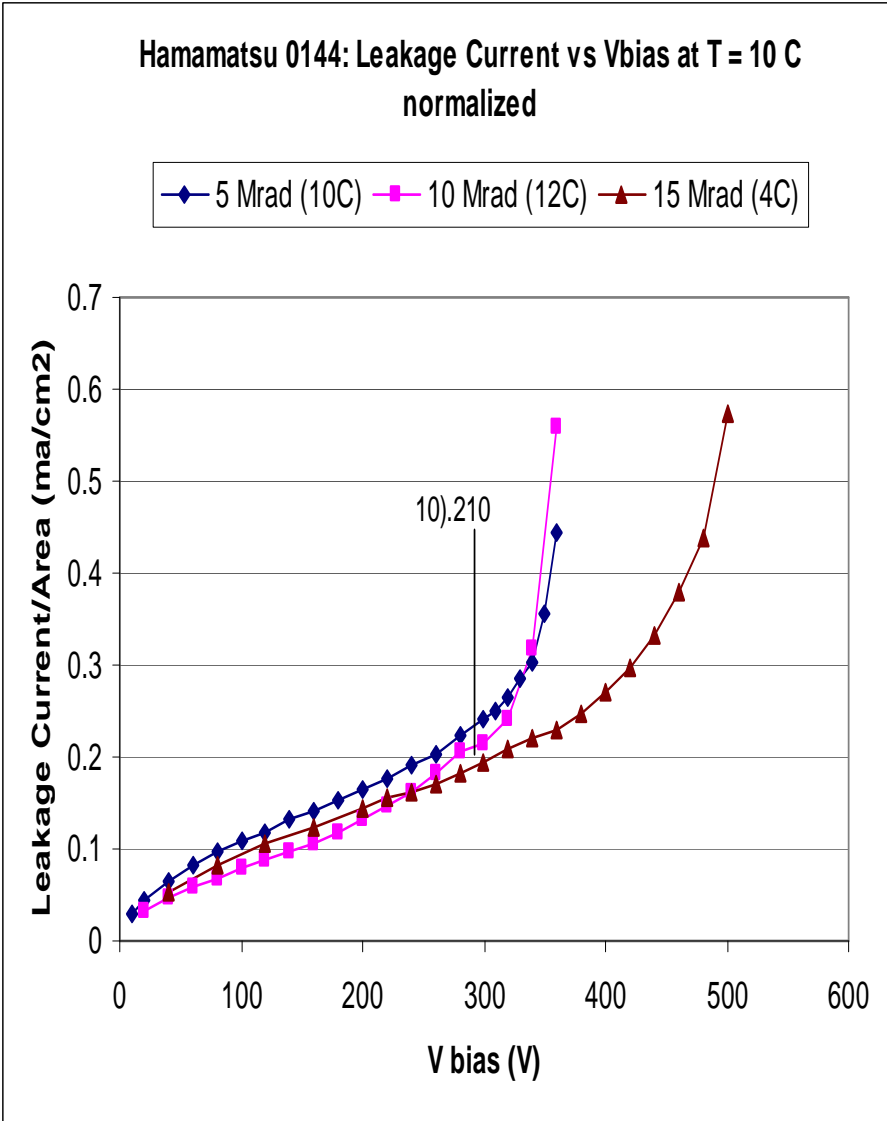
Figure 25: The leakage current per area measured as a function of applied bias voltage after irradiation of 5Mrad, 10Mrad, and 15Mrad for the HMM0144 sensor. The vertical lines indicate the measured depletion voltages with the leakage current values listed beside them.
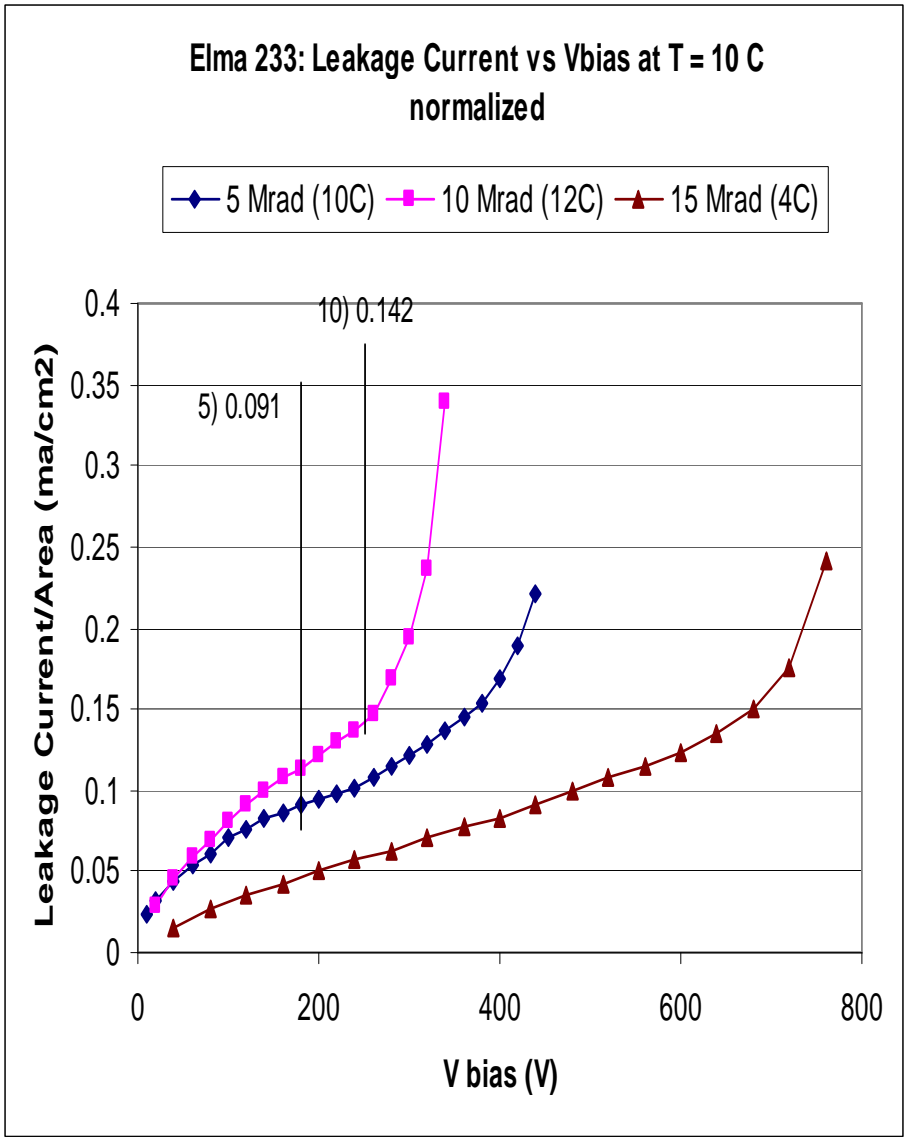
Figure 26: The leakage current per area measured as a function of applied bias voltage after irradiation of 5Mrad, 10Mrad, and 15Mrad for the ELMA 233 sensor. The vertical lines indicate the measured depletion voltages with the leakage current values listed beside them.
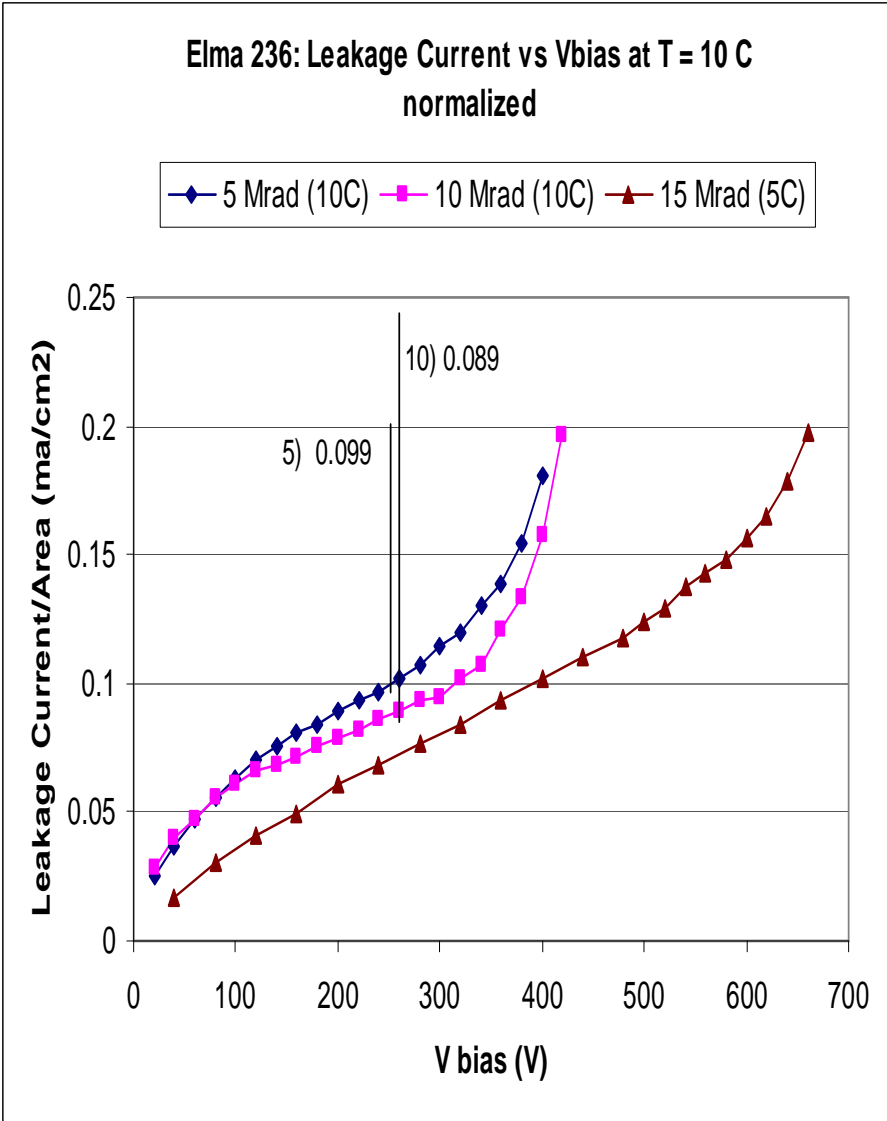
Figure 27: The leakage current per area measured as a function of applied bias voltage after irradiation of 5Mrad, 10Mrad, and 15Mrad for the ELMA 236 sensor. The vertical lines indicate the measured depletion voltages with the leakage current values listed beside them.
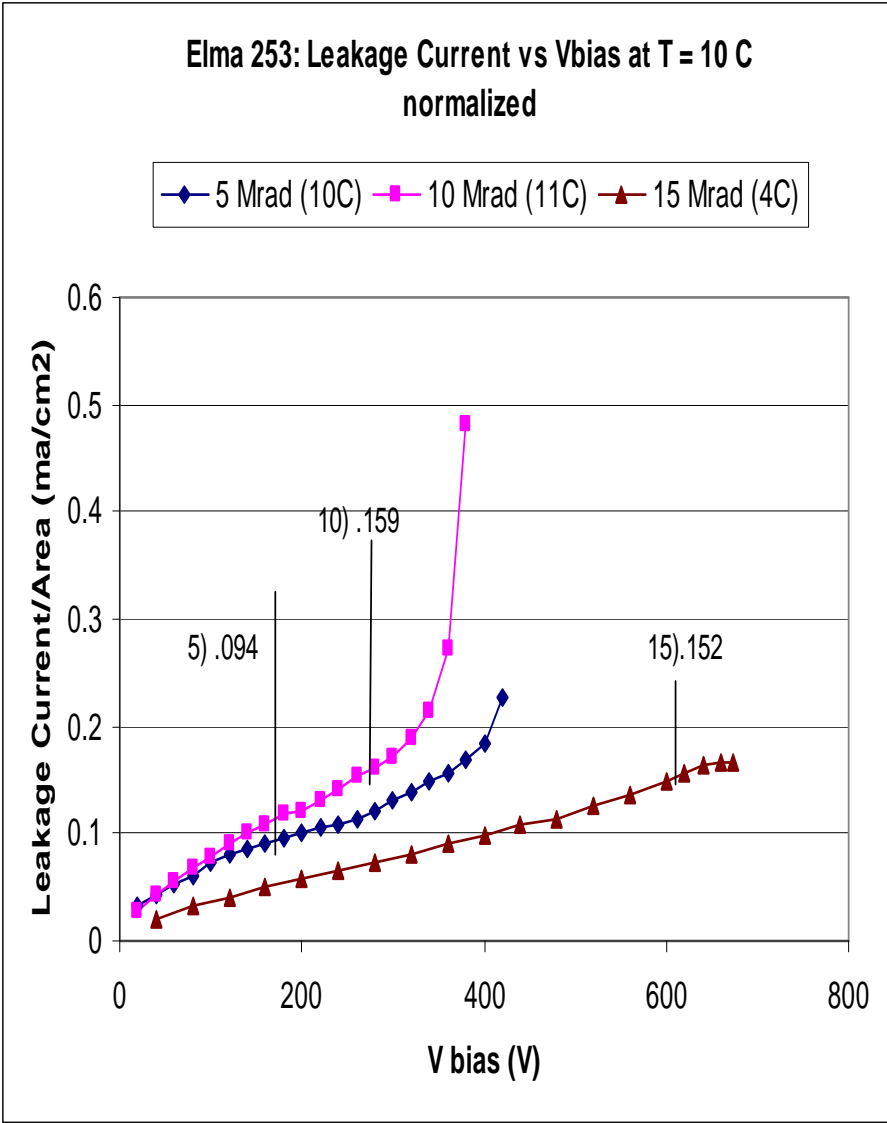
Figure 28: The leakage current per area measured as a function of applied bias voltage after irradiation of 5Mrad, 10Mrad, and 15Mrad for the Elma 253 sensor. The vertical lines indicate the measured depletion voltages with the leakage current values listed beside them.
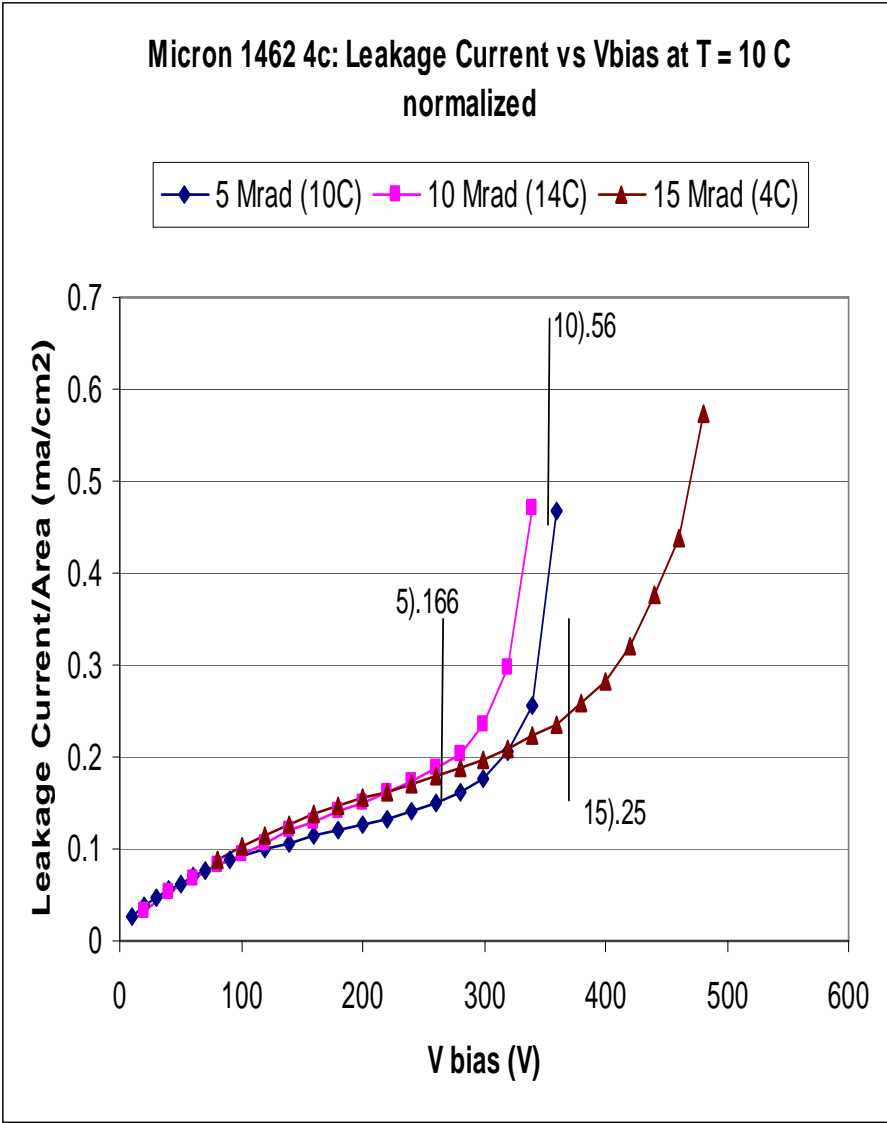
Figure 29: The leakage current per area measured as a function of applied bias voltage after irradiation of 5Mrad, 10Mrad, and 15Mrad for the Micron 1462 4C sensor. The vertical lines indicate the measured depletion voltages with the leakage current values listed beside them.
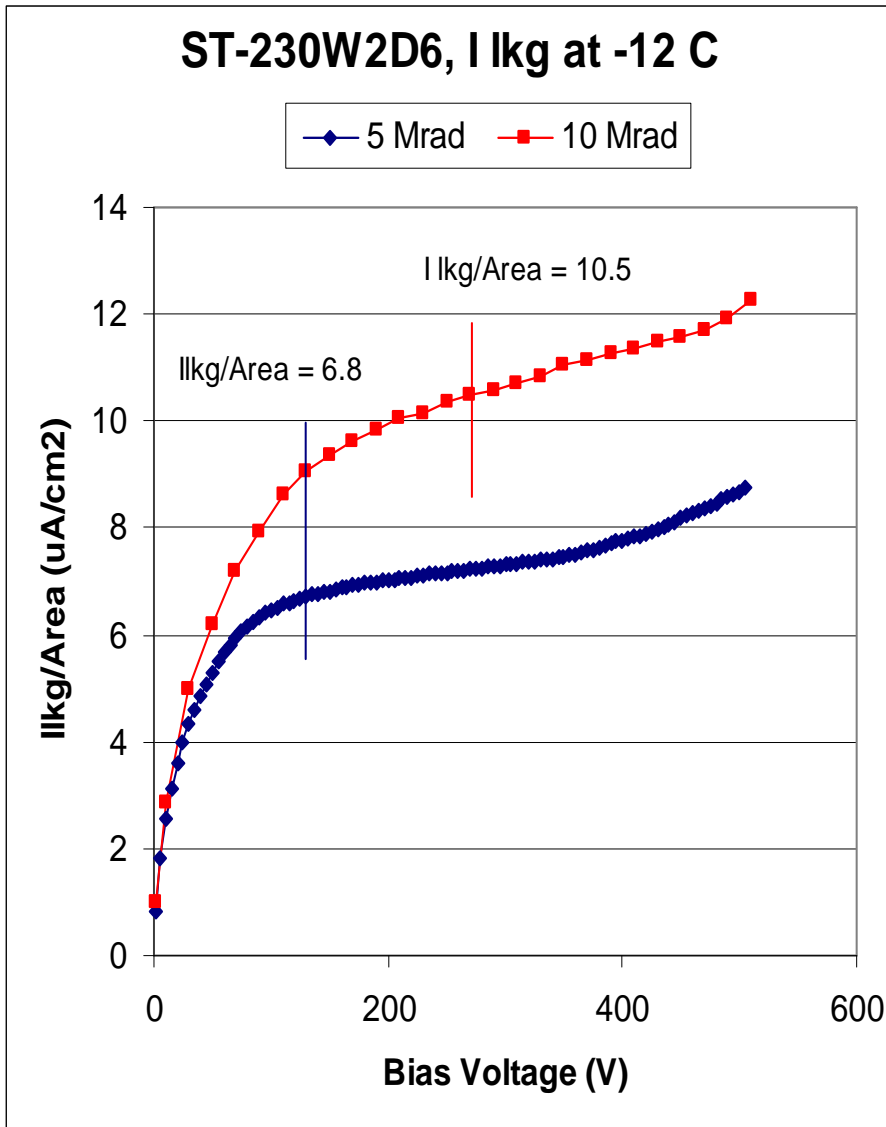
Figure 30: The leakage current per area measured as a function of applied bias voltage after irradiation of 5Mrad and 10Mrad, for the ST 230W2D6 sensor. The vertical lines indicate the measured depletion voltages with the leakage current values listed beside them.

irradiation (Mrad)	0 (nA/cm^2)		5 (mA/cm^2)		10 (mA/cm^2)		15 (mA/cm^2)	
error source	Vdep	Temp	Vdep	Temp	Vdep	Temp	Vdep	Temp
Hamamatsu 0077	0.2	0.6	0.12	0.04	0.12	0.05	0.13	0.06
Hamamatsu 0134	3.	15.	0.02	0.03	0.16	0.08	0.07	0.05
Hamamatsu 0144	1.5	6.	none	none	0.016	0.04	none	none
Elma 233	0.02	0.17	0.011	0.015	0.013	0.02	none	none
Elma 236	0.04	0.17	0.011	0.017	0.005	0.015	none	none
Elma 253	0.05	0.8	0.013	0.016	0.016	0.03	0.03	0.03
Micron 1462 4c	1.5	5.	0.03	0.03	0.17	0.10	0.04	0.04
ST230W2D6	0.04	0.04	0.001	0.009	0.002	0.015	none	none

Table 3: Leakage current errors from depletion voltage and temperature uncertainty. (Note that leakage current units are in nA for 0 Mrad and mA for 5, 10 and 15 Mrad.)

constant is a part of the description of the effective impurity concentration, N_{eff}, dependent only on fluence. Taking into account everything, N_{eff} is how effectively doped the silicon is with impurities. These impurities create acceptors and donors and are responsible for charge collection. If annealing isn't a factor, the slope of N_{eff} approaches that of g_c at high fluence. Because of this, g_c can be determined. However, a lack of measurements at low fluence, between 0 and 5 MRad, prevents N_{eff} from being studied further.

The depletion voltage is directly dependent on the absolute value of the effective impurity concentration, N_{eff},

$$V_{dep} = \frac{ed^2}{2\epsilon\epsilon_o}|N_{eff}| \qquad (6)$$

where $\epsilon = 11.5 \pm 0.5$ is the relative permittivity of the silicon and d = 300 ± 10 microns is the thickness. Therefore, for a given detector, N_{eff} can be related to V_{dep} by a simple constant. For all the detectors tested, this is

$$V_{dep} = (7.1 \pm 0.5) * 10^{-11}(Vcm^3)N_{eff} \qquad (7)$$

where N_{eff} is the effective impurity concentration and can be modeled to

$$N_{eff}(\phi, t) = N_{eff,0} - N_c(\Phi) - N_a(\Phi, t) - N_y(\Phi, t) \qquad (8)$$

Here $N_{eff,0}$ is the original doping concentration and N_c is the stable radiation induced doping concentration.

$$N_c(\Phi) = N_{c0}(1 - exp(-c\,\Phi)) + g_c\,\Phi \qquad (9)$$

The first term, $N_{c,0}$, describes the compensation of the original donor concentration. $N_{c,0}$ is determined through the ratio of $N_{c,0}$ to N_{eff}, which is set to 0.66 ± 0.15 in this study. The first term of N_c, therefore, is initially zero and converges to N_{c0} at a rate dependent on c. c is taken to be approximately $1 * 10^{-13}$, which is large enough to make the first term converge to N_{c0} well before 5 Mrad. The second term models the introduction of acceptor like states and depends directly on fluence.

N_a is for short term beneficial annealing. This is from the annealing of acceptors with time and has a self corrective effect. The end result is a reduction in depletion voltage.

$$N_a = g_a \, exp(\frac{-t}{\tau_a}) \, \Phi \qquad (10)$$

In the exponent, t is the annealing time and τ_a is a time constant found from

$$\tau_a = 70 * exp(-0.175 \, T) \qquad (11)$$

where T is the temperature in celsius and the result is time in days.

N_y is for long term reverse annealing and can be ignored if annealing time is short.

The effective impurity concentration, N_{eff}, is plotted (using the depletion voltage measurements) as a function of fluence and fitted to obtain g_c. Annealing time was assumed to be short enough to ignore long term reverse annealing. Therefore, Equation 8 for N_{eff} can be shortened to Equation 12 below

$$N_{eff}(\phi, t) = N_{eff,0} - N_c(\Phi) - N_a(\Phi, t) \qquad (12)$$

which is,

$$N_{eff}(\phi, t) = N_{eff,0} - g_c \, \Phi - N_{co}(1 - exp(-c \, \Phi)) - g_a \, exp(\frac{-t}{\tau_a}) \, \Phi \quad (13)$$

with $N_{eff,0}$ set to the initial impurity concentration found from the depletion voltage using Equation 6. All parameters are assigned the fixed values in Table 4 except for g_c. The data is fit, using a minimization to a χ^2 fit, with the TMinuit class in Root. [8]

parameter	value
g_a	$1.8 \; cm^{-1}$
$\tau_a(T = 23.9°C)$	25.6 hours
time at $23.9°C$	30 ± 10
$N_{co}/Neff, o$	0.66 ± 0.15
c	$9.60 * 10^{-14} cm^2$

Table 4: fit parameters

This measurement of g_c requires accurate knowledge of both the fluence and annealing. Uncertainty in the fluence from the proton booster

detector	$g_c (cm^{-1}) \pm (stat.) \pm (syst.)$	$g_c (cm^{-1}) \pm (combined)$
Hamamatsu 0077	$0.0061 \pm 0.0012 \pm 0.0023$	0.006 ± 0.003
Hamamatsu 0134	$0.0076 \pm 0.0008 \pm 0.0029$	0.008 ± 0.003
Elma 253	$0.0067 \pm 0.0013 \pm 0.0021$	0.007 ± 0.003
Micron 1462 4c	$0.0067 \pm 0.0007 \pm 0.0023$	0.007 ± 0.002
Weighted Average		0.007 ± 0.003

Table 5: Results on g_c found from fits of the effective doping concentration as a function of fluence.

detector	g_c at $t = 20$hrs	g_c at $t = 40$hrs	error on g_c
Hamamatsu 0077	0.0034	0.0079	0.0023
Hamamatsu 0134	0.0047	0.0104	0.0029
Elma 253	0.0045	0.0087	0.0021
Micron 1462 4c	0.0040	0.0086	0.0023

Table 6: Values of g_c found using fits where the annealing time has been varied to determine the systematic error from this source.

beam was estimated to be $\pm 10\%$. This takes into account both uncertainty in the protons per pulse and nonuniformity of radiation distribution. Also, based on records of time spent at various temperatures, it has been estimated the detectors have spent 30 ± 10 equivalent hours at room temperature (T = 23.9 C). This includes the entire time spent after the first irradiation. Time spent at lower temperatures can be normalized to an equivalent time at room temperature using the relation

$$\frac{time\ at\ T}{\tau_s\ (T)} = \frac{time\ at\ 23.9\ C}{\tau_s\ (23.9\ C)} \qquad (14)$$

Table 5 gives the values of g_c found from these fits. Figure 31, Figure 32, Figure 33, and Figure 34 show each of the fits to the effective doping concentration as a function of fluence. The overall statistical error is found from the fit. Here, uncertainties from both the depletion voltage and beam luminosity are already included. The systematic errors are described below. To obtain the final error, the statistical and systematic errors are combined in quadrature. We find the average of these four measurements weighting them by their statistical errors.

We estimate two sources of systematic errors: those due to the uncertainty in annealing time, and those due to the value of $N_{co}/N_{eff,0}$ used in the fit. The largest source of systematic error comes from the uncertainty in annealing time. To estimate this uncertainty, the data was fit using times of 20 and 40 hours. Although errors are not symmetric about the mean, they are approximately so. Therefore, error is taken as $\pm$ the difference in g_c divided by 2. The results of these fits are given in Table 6. To obtain the systematic error from $N_{co}/N_{eff,0} = 0.66 \pm 0.15$, the $\pm 1\sigma$ points are used (0.51 and 0.81), see Table 7.

The resulting stable fluence constants are consistent with each other
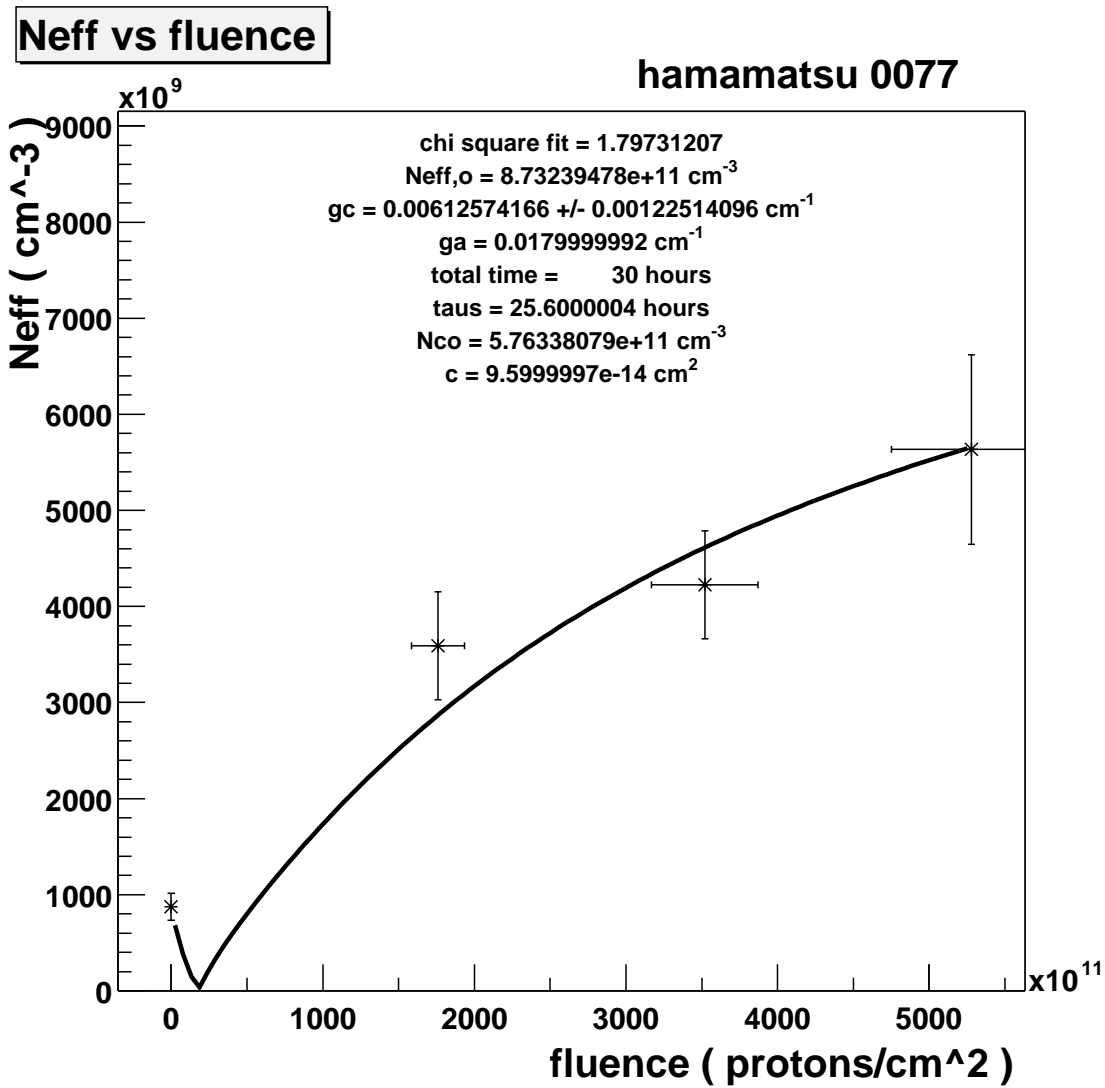
Figure 31: Fit for g_c using the effective doping concentration as a function of fluence for Hamamatsu 0077.
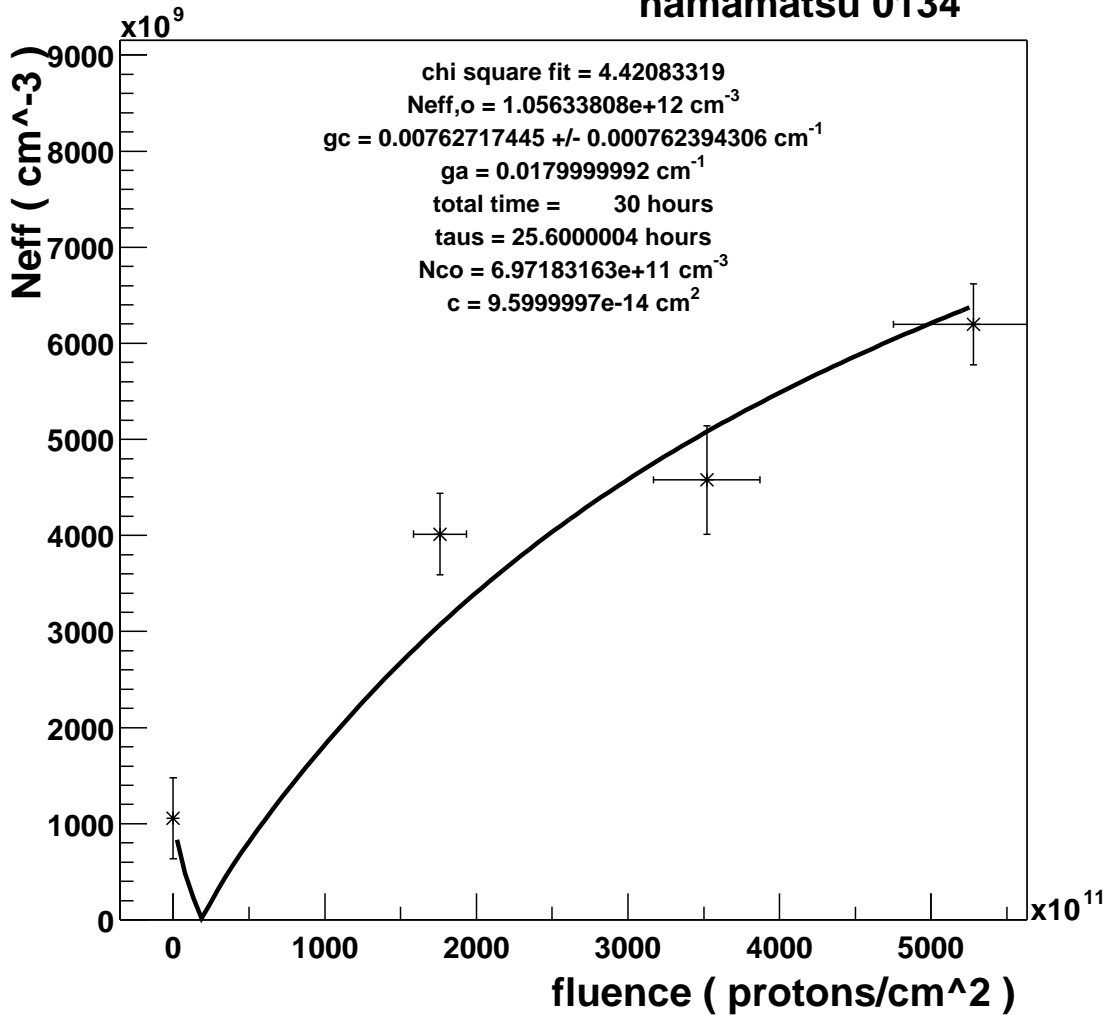
Figure 32: Fit for g_c using the effective doping concentration as a function of fluence for Hamamatsu 0134.

Neff vs fluence

elma 253

x10^9

Neff (cm^-3)

chi square fit = 10.1775092
Neff,o = 3.80281717e+11 cm^{-3}
gc = 0.00672265536 +/- 0.00134102283 cm^{-1}
ga = 0.0179999992 cm^{-1}
total time =   30 hours
taus = 25.6000004 hours
Nco = 2.50985943e+11 cm^{-3}
c = 9.5999997e-14 cm^2

x10^{11}

fluence (protons/cm^2)
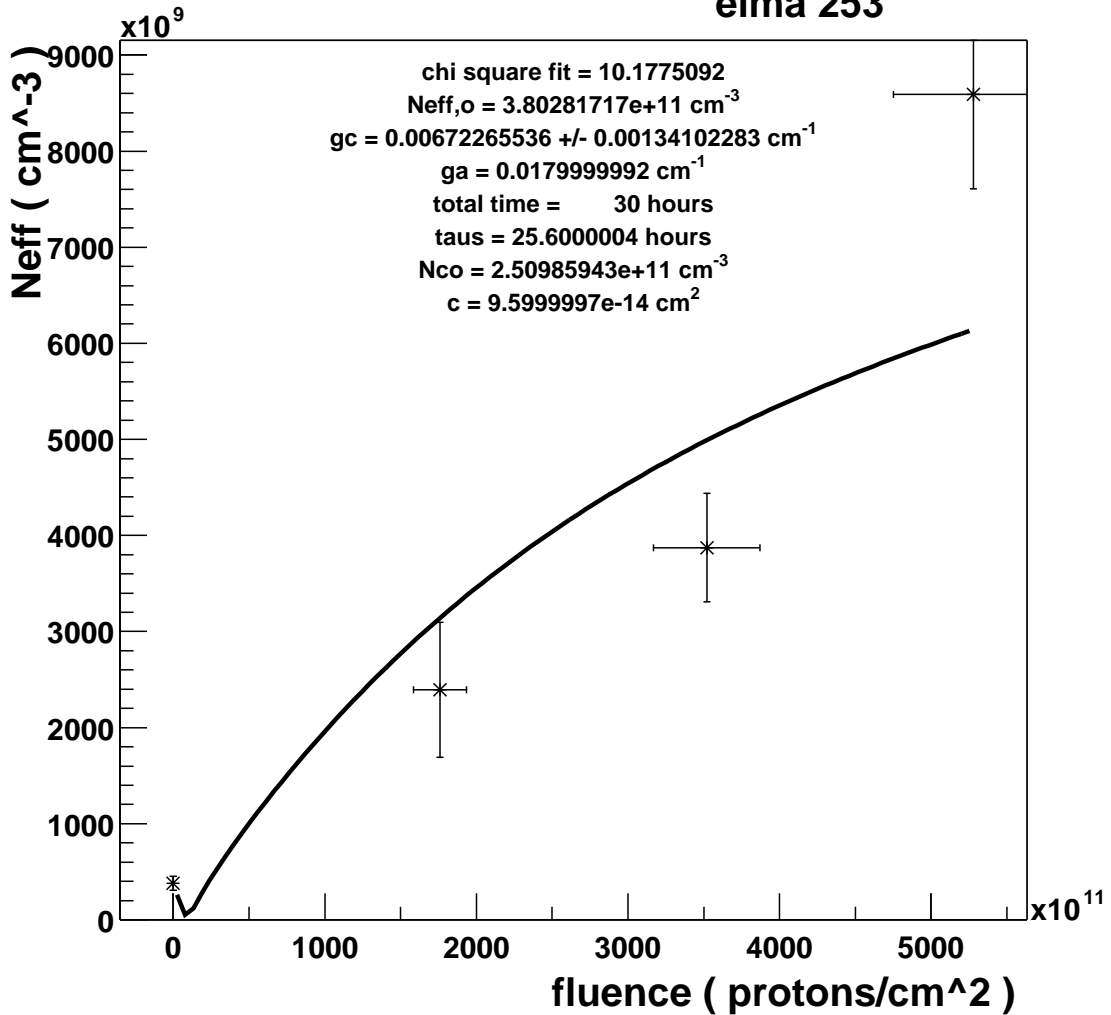
Figure 33: Fit for g_c using the effective doping concentration as a function of fluence for Elma 253.

Neff vs fluence

micron 1462 4c

chi square fit = 3.08470066
Neff,o = 1.38028175e+12 cm^{-3}
gc = 0.00669135916 +/- 0.000748255513 cm^{-1}
ga = 0.0179999992 cm^{-1}
total time =   30 hours
taus = 25.6000004 hours
Nco = 9.10985988e+11 cm^{-3}
c = 9.5999997e-14 cm^{2}
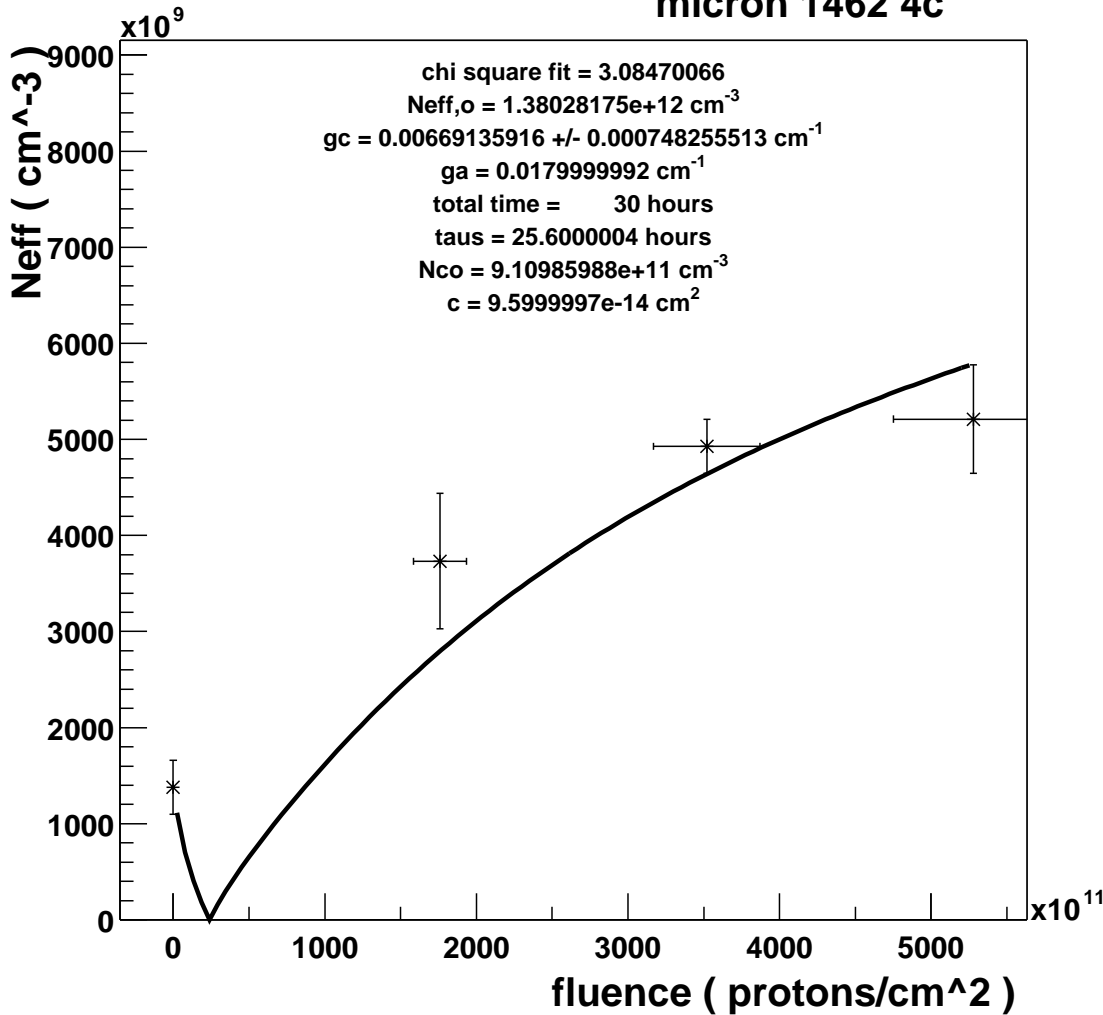
Figure 34: Fit for g_c using the effective doping concentration as a function of fluence for Micron 1462 4C.

Detector	g_c $N_{co}/N_{eff,0} = 0.51(cm^{-1})$	g_c $N_{co}/N_{eff,0} = 0.81(cm^{-1})$	error on g_c
Hamamatsu 0077	0.0065	0.0057	0.0004
Hamamatsu 0134	0.0080	0.0072	0.0004
Elma 253	0.0069	0.0066	0.0002
Micron 1462 4c	0.0073	0.0061	0.0006

Table 7: Values of g_c in cm^{-1} found using fits where the values of $N_{co}/N_{eff,0}$ (cm^{-1}) have been varied and the systematic error on g_c from this source.

and with expectations. As a comparison, the g_c found in [6] is approximately 0.017 using non radiation hard silicon. The value for g_c found in this study is smaller by a factor of 3 as is expected for radiation hard silicon. The value of g_c for standard silicon is 0.019 cm^{-1} while for oxygenated it falls to 0.0053 cm^{-1}. [3]

The radiation damage coefficient α can be determined from fitting the measured leakage currents as a function of fluence using Equation 2. Typically, $\alpha = (3 - 4) \times 10^{-17} A/cm$ at room temperature. [4] We determined the value α for the three full size detectors that we determined g_c. For the fits, the leakage per volume is found by dividing by the detector thickness (which was 300 microns) for all detectors. Figure 35, Figure 36, and Figure 37 show these fits. Table 8 gives the results of these fits. The errors are dominated by the fluctuation in the temperature. Using the weighted value, we find $\alpha = (2.2 \pm 0.2) \times 10^{-17}$. This is below the canonical value of $(3 - 4) \times 10^{-17}$ indicating that these sensors are performing well with radiation. For the smaller Elma sensors, we have also done a combined fit to find α. Figure 38 shows the result of this fit with the value of α listed in Table 8.

detector	$\alpha(A/cm^3)$
Hamamatsu 0077	$(2.5 \pm 0.7) \times 10^{-17}$
Hamamatsu 0134	$(2.6 \pm 0.5) \times 10^{-17}$
Micron 1462 4c	$(2.0 \pm 0.3) \times 10^{-17}$
Weighted Average	$(2.2 \pm 0.2) \times 10^{-17}$
Elma Average	$(1.29 \pm 0.18) \times 10^{-17}$

Table 8: The α values found from a fit of the leakage currents as a function of fluence. The weighted average has been calculated using the full size sensors.

6   Conclusions

Eight prototype Run2b silicon sensors were irradiated at the Fermilab RDF facility. The depletion voltage and leakage current was measured before irradiation and after irradiations of 5Mrad, 10Mrad, and 15Mrad.
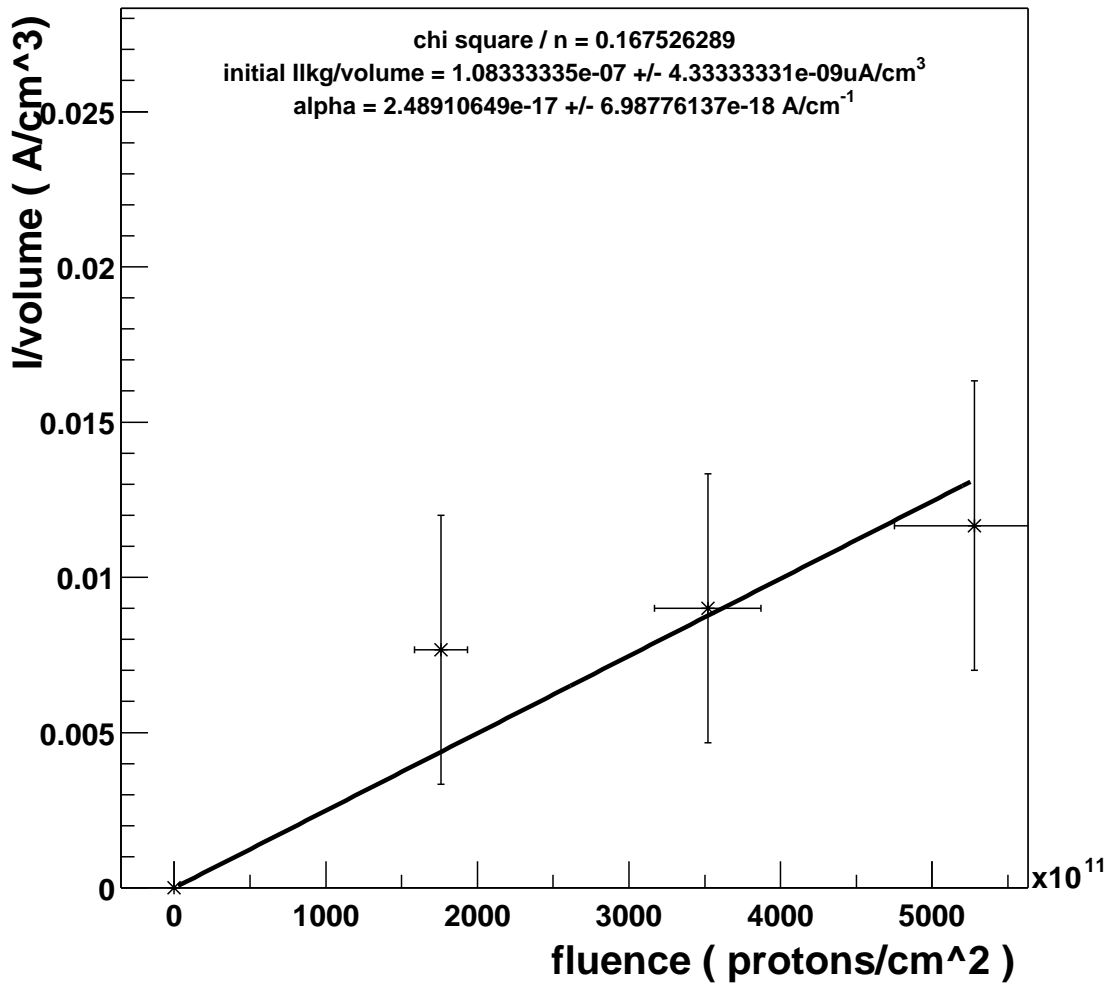
Figure 35: Fit for α using leakage current as a function of fluence for Hamamatsu 0077.
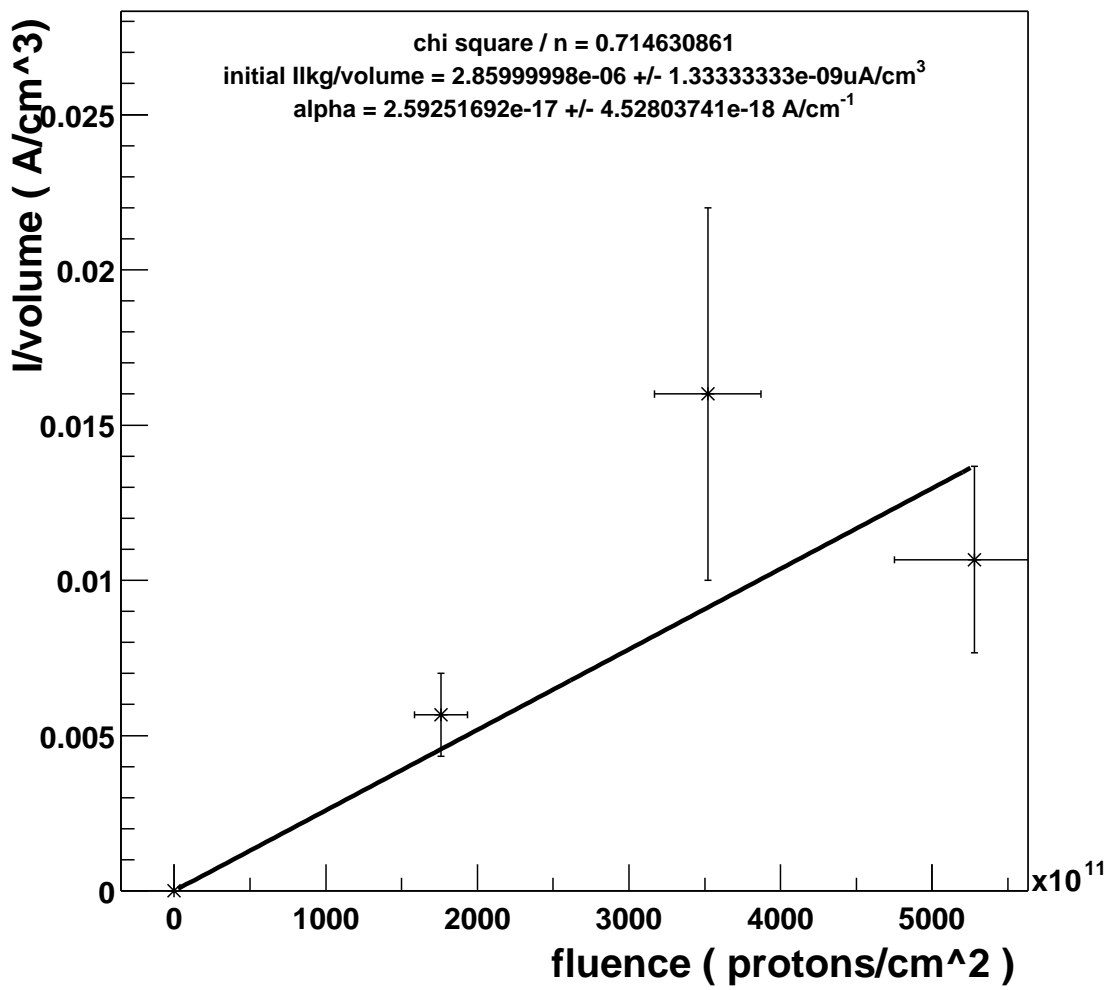
Figure 36: Fit for α using leakage current as a function of fluence for Hamamatsu 0134.

I lkg/volume vs fluence

micron 1462 4c
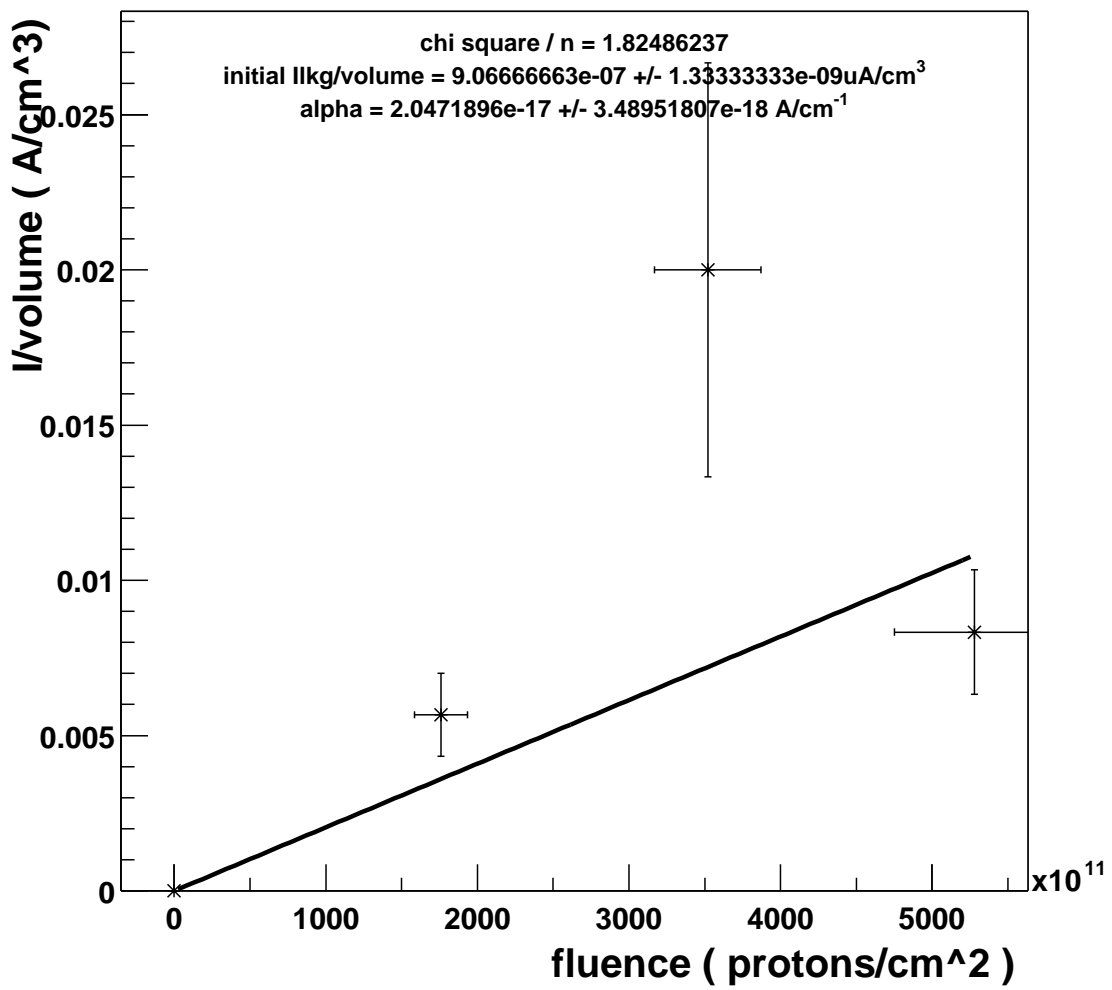
chi square / n = 1.82486237
initial Ilkg/volume = 9.06666663e-07 +/- 1.33333333e-09uA/cm^3
alpha = 2.0471896e-17 +/- 3.48951807e-18 A/cm^{-1}

Figure 37: Fit for α using leakage current as a function of fluence for Micron 1462 4C.
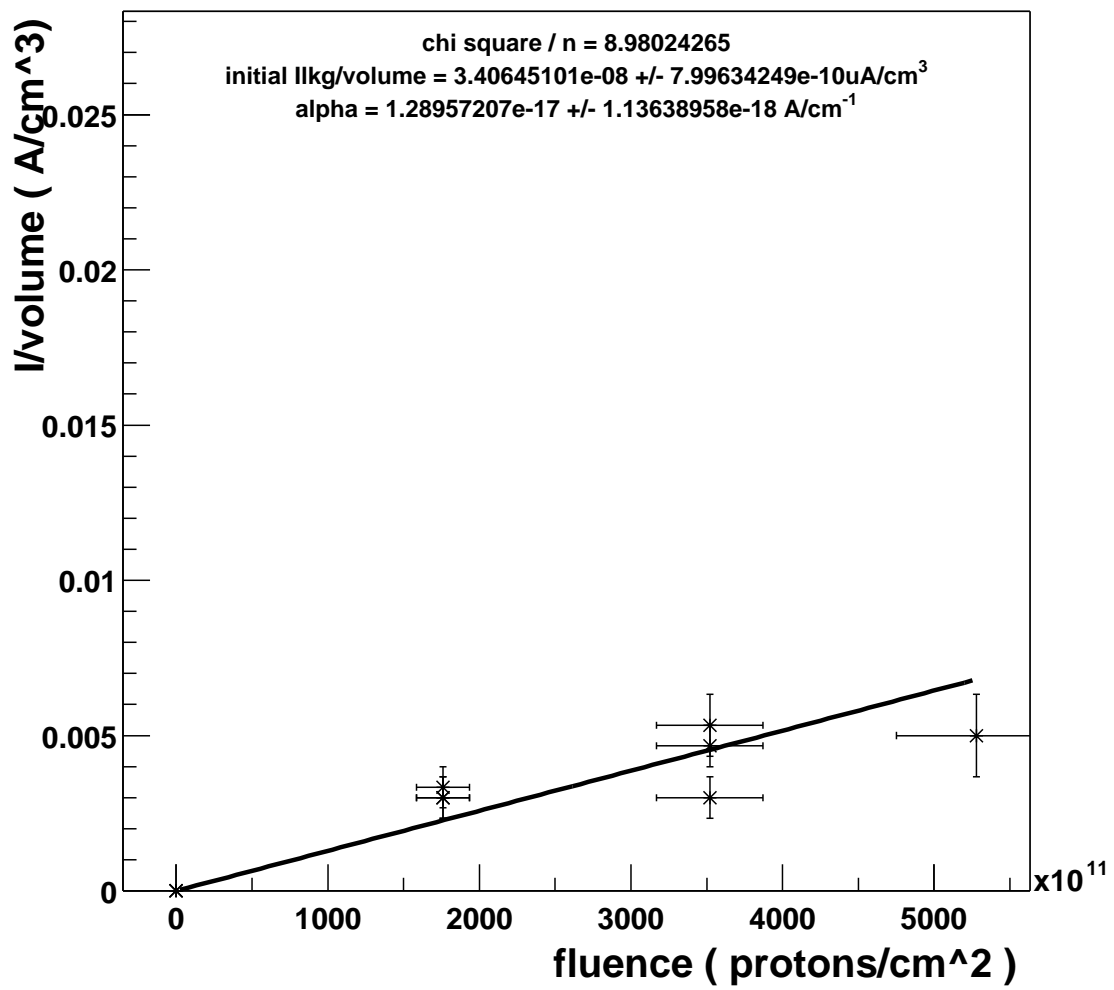
Figure 38: Fit for α using leakage current as a function of fluence for all Elma sensors.

The devices behave roughly as expected, although there is a considerable spread in the depletion voltage at 15MRad. The Elma detectors which are fabricated using a crystal orientation of $< 111 >$ have the worst behavior. The spread in depletion voltage is consistent with the variations among silicon types and manufacturers observed by LHC experiments. [9] Our estimates, supported by these results, show that these sensors will be able to withstand the radiation dose equivalent of more than $15fb^{-1}$ with significant safety margin in layers 0-5. The depletion voltage for Layer 0 sensors is expected to reach 300V for the assumed Tevatron Run2b scenario. The layer 0 and 1 sensors will be specified to break down not earlier than 700V, providing enough flexibility in overbiasing these detectors.

Leakage currents were measured at a few temperatures and found to be consistent with expectations. The breakdown voltage depends on operating temperature as well as annealing time after the intense irradiation. None of the devices showed breakdown before full depletion. We believe that additional operating margin is available at our expected operating temperature of $-10°C$.

We have measured the stable fluence constant g_c and the radiation damage slope α using four of the sensors. By fitting to the effective doping concentration as a function of fluence we find $g_c = 0.007 \pm 0.003$ which is consistent with values expected from radiation hard silicon devices. We find $\alpha = (1.61 \pm 0.14) \times 10^{-17}$ which is below the canonical value of $3 - 4 \times 10^{-17}$ indicating that our detectors are performing well with radiation.

Problems that we found with the measurements limited our accuracy. For future measurements, we will: measure the depletion voltage to higher values for all radiation doses, better control the temperature of our sensors for leakage current tests, and verify the time since irradiation to better than one hour.

We would like to acknowledge the people who helped to setup the Radiation Damage Facility at Fermilab who are not listed as authors on this paper, including Leonard Spiegel.

7 REFERENCES

References

[1] D0 Run2b silicon group, "D0 Run 2B Silicon Detector Upgrade Technical Design Report", 2002.

[2] S.Y. Choi and F. Lehner, "What do we know about radiation damage in silicon detectors?", D0 Note 3803

[3] The ROSE Collaboration, Nucl. Instr. & Meths. **A362** (1995) 297-314; RD 48 3rd Status Report (http://rd48.web.cern.ch/RD48/)

[4] F. Lehner, "New Leakage Current, Noise and Depletion Voltage Expectations for Run IIb", D0 Note 3959.

[5] J. Gardner *et al.*, "Results from Irradiation Tests on D0 Run 2a Silicon Detectors at the Radiation Damage Facility at Fermilab",D0 Note 3962.

[6] S. Lager, "Proton-Induced Radiation Damage in Double Sided Silicon Diodes", Master's Thesis, Stockholm University,Sweden, http://www.physto.se/ p98sla/projekt.html.

[7] F. Rizatdinova, "Laser test of silicon detectors at D0," D0Note 3832.

[8] ROOT Data Analysis Framework (http://root.cern.ch/root/)

[9] S. Braibant et al., "Investigation of design parameters and choice of substrate resistivity and crystal orientation for the CMS silicon microstrip detector," The CMS Experiment, CMS NOTE 2000/011.